may be inferred from the ratio $\sigma^a_\lambda/\sigma_{ext,\lambda}$ derived from SAGE I data over the South Pole. Figure 6.9 shows the annual variation of weekly averages of this extinction ratio at the South Pole. The aerosol extinction maxima that occur during the winter months indicate the presence of stratospheric clouds between about 10–17 km. These episodes of high extinction coincide with stratospheric temperatures colder than about 190 K, a factor considered important to the formation of polar stratospheric clouds and, in turn, to the chemistry responsible for the destruction of atmospheric ozone.

Another demonstration of the value of these data is given in Fig. 6.10 in the form of a six–year time series of weekly averaged aerosol optical depths integrated from 200 mb upward over the Arctic (dashed) and Antarctic (solid) regions. This time series indicates the regular appearance of polar stratospheric clouds in the Antarctic and the lack of these clouds over the Arctic. Also evident is the general increase of stratospheric aerosol over both poles after the El Chichon volcanic eruption.

Not only can SAGE detect volcanic clouds, but observations from SAGE also allow us to map their movement as they are dispersed by the stratospheric winds. Plate 1 (refer to the front of the book) shows a map of the optical depth derived by integrating the 1.02 μm SAGE extinction profiles from 2 km above the tropopause to the highest level of observation for the period in 1991 from mid–June to late July. This map highlights regions where optical depths exceed 0.1 and shows how the Pinatubo volcanic cloud has spread around the equatorial region into both hemispheres (McCormick and Viega, 1992). The line profiles below the SAGE map are the vertical profiles of lidar backscatter (a topic discussed more in Chapter 8) which were measured at Aspendale, Australia, during the same time as SAGE observations. These shows accentuated levels of backscatter between 20 and 24 km associated with the Pinatubo ash cloud.

6.3 Scattering as a Source of Radiation

So far we have only considered scattering as a process that removes photons from a particular direction such as along an instrument's line–of–sight. The radiative transfer equation used in extinction–based retrievals described earlier assumes only single scattering which is reasonable for tenuous scattering media. In dense clouds or under highly turbid skies, photons from the sun can actually reappear again along the direction of the sun when scattered

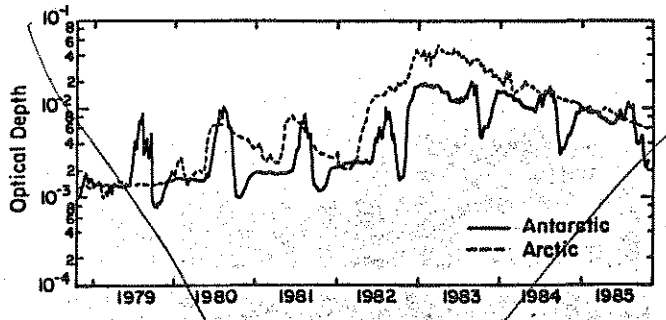

Figure 6.10 Weekly averaged optical depths integrated upward from 200 mb obtained from SAM II obsekvations. The solid line represents Antarctic measurements; the dashed represents Arctic measurements (McCormick and Trepte, 1987).

a multiple of times. In fact, many scattering problems of interest to the atmospheric sciences have to deal with multiple scattering. Multiple scattering of sunlight, for instance, gives rise to many observable phenomena that cannot be explained from single scattering arguments alone. Single scattering predicts a sky that is of uniform brightness and color contrary to what we observe. The whiteness and brightness of clouds is also a result of multiple scattering. Reflection of visible and microwave radiation from various surfaces is largely a product of multiple scattering. Multiple scattering is thus relevant to many topics of remote sensing, and especially to methods based on reflected sunlight.

To account for multiple scattering, we need to introduce a mathematical expression for the reappearance of photons along a specified direction. Unfortunately, to do so requires that we pay more attention to what we mean by direction so that we can talk about changes in direction that occur after a scattering event. We do this using a frame of reference as a basis and describe all scattering processes relative to this frame of reference. Discussion of a particular type of frame of reference used here, and the general definition of a direction vector set on this framework, is relegated to Appendix 1. A few exercises to familiarize the reader with these geometric concepts are

intensities at adjacent wavelengths λ_1 and λ_2. We represent these measurements by I_1 and I_2 and it follows from (7.11) that

$$I_1 = \mathcal{B}_1(T_s)\mathcal{T}_1(\tau_1^*, \mu) + \mathcal{B}_1(T_a)[1 - \mathcal{T}_1(\tau_1^*, \mu)] \tag{7.13a}$$

$$I_2 = \mathcal{B}_2(T_s)\mathcal{T}_2(\tau_2^*, \mu) + \mathcal{B}_2(T_a)[1 - \mathcal{T}_2(\tau_2^*, \mu)] \tag{7.13b}$$

Prabhakara et al. (1974) claim that the value of T_a varies by less than 1 K across the 10.5–12.5 μm window so it is also reasonable to assume a common value for T_a. It is also reasonable to expect that the surface emissivities are the same at adjacent wavelengths (here we conveniently assume this emissivity to be unity).

To solve for T_s, we make use of Taylor's theorem to arrive at the following

$$\mathcal{B}_\lambda(T) \approx \mathcal{B}_\lambda(T_a) + \frac{\partial \mathcal{B}_\lambda}{\partial T}(T - T_a)$$

where the partial derivative is evaluated at $T = T_a$. Application of this equation to both wavelengths and further elimination of the $T - T_a$ factor yields

$$\mathcal{B}_2(T) \approx \mathcal{B}_2(T_a) + \frac{\partial \mathcal{B}_2/\partial T}{\partial \mathcal{B}_1/\partial T}[\mathcal{B}_1(T) - \mathcal{B}_1(T_a)] \tag{7.15}$$

We use this expression twice, once to approximate our observation I_2, which we write in terms of a brightness temperature $T_{b,2}$ according to $I_2 = \mathcal{B}_2(T_{b,2})$, and a second time to approximate $\mathcal{B}_2(T_s)$ to obtain

$$\mathcal{B}_1(T_{b,2}) = \mathcal{B}_1(T_s)\mathcal{T}_2 + \mathcal{B}_1(T_a)[1 - \mathcal{T}_2] \tag{7.16}$$

Eliminating $\mathcal{B}_1(T_a)$ from (7.13a) and (7.16) yields the split–window equation

$$\mathcal{B}_1(T_s) = I_1 + \eta[I_1 - \mathcal{B}_1(T_{b,2})] \tag{7.17}$$

where

$$\eta = \frac{1 - \mathcal{T}_1}{\mathcal{T}_1 - \mathcal{T}_2} \tag{7.18}$$

This relationship is further approximated and linearized in terms of the brightness temperatures,

$$T_s \approx T_{b,1} + \eta[T_{b,1} - T_{b,2}] \tag{7.19}$$

In practice, the actual split–window technique is rarely used in the form given by either (7.17) or (7.19) but these serve merely as a justification for regressing the surface temperature as a linear function

of the measured brightness temperatures. The more typical form of this regression is

$$SST = aT_{11} + b(T_{11} - T_{12}) - c \tag{7.20}$$

where the coefficients a, b, and c are empirically derived from in situ observations such as obtained from drifting buoys. In this expression, $T_{11,12}$ are the brightness temperatures of the $11\mu m$ and $12\mu m$ channels of the AVHRR instrument. When comparing the satellite observations to conventional observations, it is important to note that the satellite temperatures correspond to the temperature of a surface layer just a few millimeters thick (this is referred to as the "skin" temperature). In situ measurements, on the other hand, are bulk measurements of the temperature of a layer of water perhaps a few meters deep. The regression approach of the MCSST is an attempt, in part, to tune the satellite skin temperatures to the in situ bulk temperature. Part of this tuning also accounts for the fact that the atmosphere is not completely transparent at the window wavelengths, especially over the moist tropics (discussion of Table 3.1 and Problem 7.6 offer more quantitative perspectives of these atmospheric effects).

The multichannel approach described here is presently used operationally by NOAA; the precise details of the operational algorithm are described by McClain et al. (1985). The approach actually uses both the $11\mu m$ and $12\mu m$ channels of the AVHRR and the $3.7\mu m$ window channel and has a form similar to that of (7.20). An important part of the algorithm, and one of relevance to many retrieval problems involving infrared emission measurements, is the need to establish whether or not clouds appear in the field of view. Undetected clouds are a source of bias when temperatures associated with the emission from clouds are mistakenly mixed with the SSTs.

Another problem associated with the MCSST approach is that the retrieval of SST is affected by other changes in the atmospheric infrared opacity that occur, for example, with increased concentrations of stratospheric aerosol from volcanic eruptions. Figure 7.5 shows a monthly time series of in situ and satellite observations for the 1982–1986 period for two eastern Pacific regions: one in the tropics (labeled Nino–3) and one in the northern midlatitudes (Namais). The satellite–derived SSTs are lower overall than are the in situ values by about 0.5 degrees; however, the bias is approximately 2 degrees during the period of the El Chichon eruption.

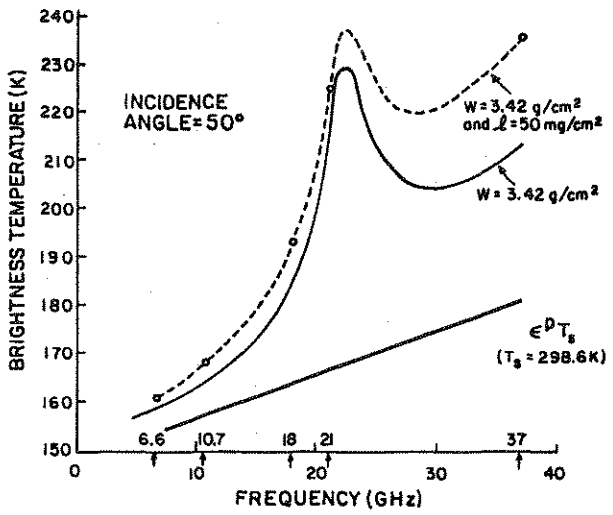

Figure 7.6 Brightness temperature spectra between 6 and 37 GHz for no atmosphere (solid line), a tropical model atmosphere with 34.2 kgm^{-2} of precipitable water (solid curve), and the addition of 0.5 kgm^{-2} of cloud liquid water (from Prabhakara et al., 1982).

ference in brightness temperature associated with the emission by cloud droplets and water vapor increases as the spectral frequency increases. Also shown for reference are the spectral positions of the channels of two satellite microwave radiometers, the Scanning Multichannel Microwave Radiometer (SMMR) flown on the experimental Nimbus 7 satellite (upward pointing arrows) and the Special Sensor Microwave Imager (SSM/I – downward pointing arrows) which has been used operationally since July 1987 as part of the Defense Military Satellite Program.

7.3.1 Microwave Radiative Transfer

It is important to realize that a significant portion of the microwave intensity emitted from the atmosphere toward the ocean surface is reflected back to the atmosphere. Furthermore, the emissivity is polarized by an amount dependent on the viewing direction (Section

4.5). Equation (7.6a) can be readily modified to account for these factors in the following way,

$$T_B = \epsilon^p T_s e^{\tau^*/\mu} + \int_0^{\tau^*} T(t) e^{-(t-\tau)/\mu} d(\frac{t}{\mu})$$

$$+\mathcal{R}^p e^{-\tau^*/\mu} \int_{\tau^*}^{0} T(t) e^{-(\tau^*-t)/\mu} d(\frac{t}{\mu}) \qquad (7.21)$$

where T_B is the brightness temperature measured at the satellite altitude,[3] T_s is the sea surface temperature, ϵ^p is the emissivity of the ocean surface with the given polarization state p, and $\mathcal{R}^p = (1 - \epsilon^p)$ is the surface reflectivity. The first term of the right-hand side of (7.21) is the surface emission term, the second defines the integrated atmosphere emission, and the third corresponds to the downwelling radiation emitted by the atmosphere, reflected at the surface and then transmitted to the satellite sensor. A simplification to (7.21) can be made if it is assumed that the absorption by water vapor is confined to the boundary layer. Thus

$$\int_0^{\tau^*} T e^{-(t-\tau)/\mu} d(\frac{t}{\mu}) \approx T_s \int_0^{\tau^*} e^{-(t-\tau)/\mu} d(\frac{t}{\mu}) \approx T_s \left(1 - e^{-\tau^*/\mu}\right) \qquad (7.22)$$

where we have specifically assumed that the emitting temperature of the water vapor is the same as the sea surface temperature. Refinements to this approximation to include vertical variations of temperature are relatively simple to make but lead only to relatively small corrections to what is presented below so these are omitted here. On substitution of (7.22) into (7.21) we obtain

$$T_B \approx T_s \left[1 - \mathcal{T}^2(\mu)(1 - \epsilon^p)\right] \qquad (7.23)$$

where $\mathcal{T}(\mu) = e^{-\tau^*/\mu}$ is the transmissivity along the direction defined by μ.

[3] We can invoke the Rayleigh–Jeans distribution for $\mathcal{B}$ for many of the microwave frequencies of interest in this book and thus replace this function simply by the temperature T (refer to the discussion in Section 2.5 for more details).

$\exp(-k_w w/\mu)$ where k_ℓ is the absorption coefficient of liquid water (the form of this coefficient is described in Section 5.3) and k_w is the absorption coefficient for vapor. With some rearrangement of (7.24), it follows that

$$k_\ell W + k_w w = -\frac{\mu}{2} \ln \frac{\Delta T_B}{T_s(\mathcal{R}^V - \mathcal{R}^H)\mathcal{T}_{oz}^2} \tag{7.25}$$

This equation, applied to both the 19 GHz and 37 GHz measurements, constitutes a set of linear simultaneous equations which can be solved for w and W given values of $\mathcal{T}_{oz,19}$, $\mathcal{T}_{oz,37}$, Δk_w, and Δk_W and modeled values of $\mathcal{R}^V$ and $\mathcal{R}^H$. These surface reflectivities are functions of wind speed as previously noted in Chapter 4.

Knowing just what values to use for the absorption coefficients is perhaps the greatest source of uncertainty not only to the retrieval described here but also to most retrievals of water vapor based on measurements of atmospheric emission. Values of k_ℓ can be taken from a number of sources and the values of k_W in principle follow from the particle scattering theories discussed in Chapter 5. The temperature dependence of k_W arising from the temperature dependence of the refractive index of water at these microwave frequencies is yet another source of uncertainty.

Examples of the precipitable water w derived from this retrieval method are given in Figs. 7.8a and b as four-year seasonal averages of w for December–January–February and June–July–August, respectively. The uncertainty in w is estimated to be about 3 kgm^{-2} based on comparisons with near coincident radiosonde data. The distribution of monthly mean w broadly follows the distribution of SST (Stephens, 1990) with the largest amount over the warmest waters of the equatorial western Pacific Ocean.

One significant factor that has limited the wide use of microwave liquid water data is the general lack of independent data to verify retrievals. Greenwald et al. (1992) attempt such a verification using a limited amount of independent ground-based microwave measurements of W as well as an estimate derived from AVHRR measurements of reflected sunlight. Comparisons between near coincident SSM/I satellite values of W with those of both AVHRR and the surface microwave measurements are presented in the form of a scatter plot in Figs. 7.9a and b, respectively, for stratocumulus clouds off the west coast of California. The error bars are meant to signify the extent of spatial variability associated with the measurements and represent one standard deviation above and below the mean value.

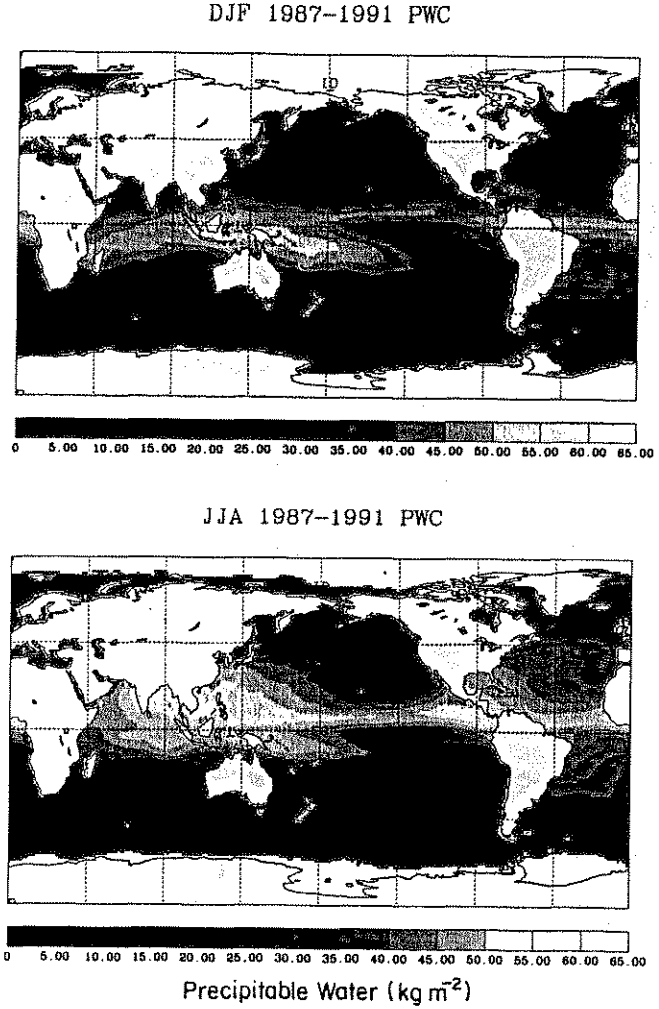

Figure 7.8 (a) The DJF averaged precipitable water derived as an average of DJFs from four years of data. (b) Same as (a) but for the JJA season (Jackson and Stephens, 1993).

ISCCP Cloud Algorithm Intercomparison

W. B. ROSSOW,* F. MOSHER,** E. KINSELLA,† A. ARKING,§ M. DESBOIS,¶ E. HARRISON,α P. MINNIS,α E. RUPRECHT,*¶ G. SEZE,‡ C. SIMMER,|| AND E. SMITH"

*NASA Goddard Space Flight Center, Institute for Space Studies, New York, NY 10025
**National Severe Storm Forecast Center, NOAA, Kansas City, MO 64106
†MA Com Sigma Data Inc., NASA/GISS, New York, NY 10025
§NASA Goddard Space Flight Center, Greenbelt, MD 20771
¶Laboratoire de Meteorologie Dynamique du CNRS, 91128 Palaisseau Cedex 05, France
αNASA Langley Research Center, Hampton, VA 23665
**Institute fur Geophysik und Meteorologie, Universitat zu Koln, 5 Koln 41, Federal Republic of Germany
‡Laboratoire de Meteorologie Dynamique du CNRS, 91128 Palaisseau Cedex 05, France
||Los Alamos National Laboratory, Los Alamos, NM 87545
"Department of Meteorology, Florida State University, Tallahassee, FL 32036

(Manuscript received 31 July 1984, in final form 5 April 1985)

ABSTRACT

The International Satellite Cloud Climatology Project (ISCCP) will provide a uniform global climatology of satellite-measured radiances and derive an experimental climatology of cloud radiative properties from these radiances. A pilot study to intercompare cloud analysis algorithms was initiated in 1981 to define a state-of-the-art algorithm for ISCCP. This study compared the results of applying six different algorithms to the same satellite radiance data. The results show that the performance of all current algorithms depends on how accurately the clear sky radiances are specified; much improvement in results is possible with better methods for obtaining these clear-sky radiances. A major difference between the algorithms is caused by their sensitivity to changes in the cloud size distribution and optical properties: all methods, which work well for some cloud types or climate regions, do poorly for other situations. Therefore, the ISCCP algorithm is composed of a series of steps, each of which is designed to detect some of the clouds present in the scene. This progressive analysis is used to retrieve an estimate of the clear sky radiances corresponding to each satellite image. Application of a bispectral threshold is then used as the last step to determine the cloud fraction. Cloudy radiances are interpreted in terms of a simplified model of cloud radiative effects to provide some measure of cloud radiative properties. Application of this experimental algorithm to produce a cloud climatology and field observation programs to validate the results will stimulate further research on cloud analysis techniques as part of ISCCP.

1. Introduction

Throughout the 1980s an international network of operational weather satellites will provide global radiance measurements in the visible (0.6 μm) and thermal infrared (11 μm) spectral intervals with a spatial resolution of at least 10 km and a time resolution of at least 3 h. In July 1983 the International Satellite Cloud Climatology Project (ISCCP) began collection of a uniform global climatology of satellite measured radiances and will derive cloud properties to characterize the distribution and variation of clouds and their effects on Earth's radiation budget (Schiffer and Rossow, 1983). The climatological data obtained by ISCCP will be key elements in the study of cloud radiative feedbacks on climate and the improvement of climate model realism (GARP, 1975, 1978; Rossow, 1981). They will also prove useful for studies of other aspects of the climate involving clouds, such as the hydrologic cycle.

Selection and application of an operational cloud algorithm for ISCCP does not imply that the best method is already available, but is meant to stimulate research on improving methods of remote sensing and analysis of cloud properties. Thus, a major component of ISCCP is a research program to validate the operational cloud climatology and develop improved methods of analysis. This validation effort is part of a larger research program to investigate cloud–climate problems employing the radiance and cloud climatologies produced by ISCCP.

ISCCP research on cloud algorithms began with a pilot study initiated in late 1981 to evaluate currently available cloud analysis algorithms, to test the effects of data volume compression schemes, and to design the operational algorithm for ISCCP (World Climate Program, 1982b). A full resolution radiance data set from GOES-East and TIROS-N was sent to ten research groups and a program of analyses and tests was defined. Four Algorithm Intercomparison Workshops were held, the First in Ottawa, 31 May–1 June 1982 (World Climate Program, 1982a), the Second and Third in New York on 9–11 December 1982 and 7–8 April 1983, respectively (World Climate Program,

1) To construct a climatology of cloud radiative properties from available satellite radiance data necessitates utilization of both the visible and infrared wavelength measurements, when available (daytime), but the algorithm must work with only infrared data (nighttime). The requirement for monitoring diurnal cloud variations over the whole globe with the same type of data currently limits the data to two spectral channels near 0.6 and 11 μm wavelengths.

2) To observe diurnal cloud variations over the whole globe and keep the total data volume manageable requires application of the algorithm to data which have degraded spatial distribution information. The algorithm must minimize sensitivity to this necessary data degradation.

3) To attain global uniformity in the climatology requires that the algorithm minimize cloud type and scene dependence in its results.

4) The behavior of the algorithm for simple and complex cases, for widely varying cloud types, and over all regions of Earth must be understood well enough to allow estimation of uncertainties.

In other words, the algorithm design described here represents compromises guided by the particular objectives of the project; *other compromises are possible.* In effect each set of choices made in designing an algorithm represents a distinct cloud model parameterizing actual cloud behavior; the particular parameterization adopted here is described in Section 6.

3. Description of pilot test

a. Data set

Collection of all of the raw imaging data from operational weather satellites would require nearly 200 000 (1600 bpi) data tapes per year for storage. This large volume is produced by high spatial resolution in visible channel images (from 1–4 km) and high time resolution (as high as every half hour). Data volume compression before analysis is clearly necessary. Since the lowest time resolution available among the current satellites is three hours, the first stage of the data compression is to reduce all satellites to three hour resolution, which has been found sufficient to describe average diurnal cloud variations (Harrison *et al.*, 1983). The volume of all the data collected every three hours is still about 50 000 tapes per year. Consequently, a second stage of the data compression is required that involves reduction of the spatial information. The pilot study data set was selected to allow study of different ways of reducing the spatial information and their effects on the cloud algorithm results.

The pilot study data set, distributed to all participants, includes both geosynchronous and polar orbiting satellite data. The GOES-East data are full resolution visible images (0.9 km resolution at nadir, 0.5–0.7 μm spectral interval) and infrared images (6.9 km resolution at nadir, 10–12 μm spectral interval) taken every three hours, starting with 0000 GMT, for 5–19 February 1979. A visible channel radiance calibration is obtained from Norton *et al.* (1980). The infrared calibration is based on the NOAA NESDIS operational technique utilizing on-board reference targets. The TIROS-N radiance measurements (4 km resolution at nadir, 0.55–0.9 μm, 0.7–1.0 μm, 3.6–4.0 μm and 10.5–11.5 μm spectral intervals) once per day are for the same geographic regions. Calibration for these radiances are those operationally provided by NOAA NESDIS (Kidwell, 1981). The data cover three geographic regions, approximately 2000 km (or 20°) square centered on the coordinates: 40°N, 75°W; (Region 1, east coast of the United States and Canada); 2.5°N, 45°W (Region 2, northern coast of Brazil); and 30°S, 72.5°W (Region 3, west coast of Chile). Each region is subdivided into 2.5° square boxes, 64 boxes covering the whole region (Fig. 1).

These regions and times were selected for study for two basic reasons. First, the three regions cover the basic climatological zones on Earth with both land and ocean areas represented: Region 1 represents winter midlatitudes with a continental east coast oceanic regime, Region 2 represents the tropical–subtropical regime including the ITCZ and trade wind regions, and Region 3 represents a subtropical–summer midlatitude region with a continental west coast oceanic regime. The most important exception to providing a complete climatological sample is the lack of a data set for a polar region; however, some relevant information is available in the analysis of the extreme northern part of Region 1. Second, the particular time period covered by the data was selected to include in Regions 1 and 3 some particularly challenging situations. Specifically, this time period includes a severe east coast snow storm followed by extremely cold, clear weather over Region 1, producing a rapidly changing set of surface conditions with both large scale cloud systems and clear skies over the land. During the same period in Region 3, the cloudiness in the Andes varies from scattered thunderstorms to a fairly large storm system over Argentina. Consequently, the results presented in Section 4 represent the performance of these algorithms applied deliberately to some of the most difficult cloud types and weather situations.

b. Cloud analysis algorithms

All cloud algorithms consist of two basic steps: cloud detection and cloud analysis. The first step partitions the observed radiance values into those representing clear scenes and those representing cloudy scenes. Different algorithms are distinguished by the logic employed to make this choice. The second step involves the quantitative determination of cloud properties from the measured radiances. This step may be as simple as counting cloudy image pixels to obtain a single cloud parameter (e.g., fractional cloud cover) or as complex

The results presented here summarize detailed intercomparisons of the six methods applied to the largest amount of data (see World Climate Program, 1984). These particular algorithms are a visible threshold method (VIS TH), an infrared threshold method (IR TH), a bispectral threshold method incorporating a radiative transfer analysis (RT TH), a hybrid bispectral threshold method (HB TH), an asymmetric Gaussian histogram analysis (AG HIS) and a dynamic cluster histogram analysis (DC HIS). The first three of these methods are threshold techniques, whereas the last two are statistical methods. The fourth method is a hybrid approach, combining some features of threshold and statistical methods. All of these algorithms are being studied as part of research projects and do not represent the same stage of development.

1) VISIBLE AND INFRARED THRESHOLD

The simplest form of the threshold method classifies all image (visible or infrared) pixels as clear or cloudy according to whether the measured radiance (R or T)[1] differs from a clear sky value (RS or TS) by more than some predetermined threshold amount (ΔR or ΔT). For visible (infrared) radiances a pixel is called cloudy if $R > \mathrm{RS} + \Delta R (T < \mathrm{TS} - \Delta T)$. The radiative model implied by this method assumes that the effects of the surface and atmosphere on the radiances are independent of time and viewing geometry to a precision determined by ΔR and ΔT. The cloud cover fraction is then given by counting the number of cloudy pixels; that is, all cloudy pixels are assumed to be 100% cloud covered. The mean clear and cloudy radiances can then be taken to represent some cloud property; namely, RC = average [R(cloudy)], RS = average [R(clear)], TC = average [T(cloudy)] and TS = average [T(clear)]. More complicated cloud radiative models can be used to derive other quantities (e.g., albedo) from the cloudy radiance values.

The two methods presented here (VIS TH and IR TH) are more involved than suggested above because of the method used to select the clear sky radiances. The clear sky and cloudy radiances are assumed to form a monotonic distribution, with the clear sky as an extremum (minimum reflectivity or maximum brightness temperature). Fifteen-day radiance time records for each pixel location are examined to find the extreme values which are then taken to be representative of clear sky for the whole 15-day period. For a geosynchronous satellite, this approach can compensate for viewing geometry effects (which do not change in time) by obtaining a clear sky radiance for each location and time of day. A spatial filter is applied to the resulting clear sky radiance map to remove "noise spikes" representing cloud contamination. For cloud detection, a threshold value representing about 3% reflectivity and 6 K in temperature is applied. Thus, for individual images, visible pixels more than 3% brighter than the clear sky or infrared pixels more than 6 K colder than the clear sky are counted as cloudy pixels. The resolution of the results from these threshold methods is limited only by the resolution of the satellite radiometer (or the data if they have been compressed by spatial averaging) and the frequency of the observations.

2) RADIATIVE TRANSFER ANALYSIS

This method (Rossow *et al.*, 1985), though in effect a threshold method, differs in two respects from the above methods. First, for daytime data, this method applies both a visible and an infrared threshold, together. In this version of the method, both thresholds must be exceeded before a pixel is counted as cloudy. (At night, this method is similar to IR TH). Second, the clear sky radiance values are derived from a combination of statistical analysis of the time record of satellite observed radiances and conventional data sources. For the results presented here, RS over land is obtained from a statistical analysis of radiances from the NOAA-5 Scanning Radiometer and RS over water is based on a theoretical reflectivity model, while TS is obtained from the NMC global temperature and humidity analysis products.

In practice, this method compares the observed radiances to radiative transfer calculations using a model of the atmosphere, surface and clouds. The atmosphere is a Rayleigh scattering gas lying above and below a single cloud layer with a vertical temperature structure defined by the daily average NMC analyses. Radiation from the sun is partially absorbed by ozone distributed according to a zonal mean, seasonal climatology based on NIMBUS-4 BUV results (Hilsenrath and Schlesinger, 1981). Land surfaces are modeled as isotropic reflectors with reflectivities that vary with location. Snow cover brightening is included for Region 1 but based on data from a different year. Ocean reflectivity is calculated from Fresnel reflection coefficients with the wave-slope statistical model of Cox and Munk (1956). All surfaces are assumed to have unit emissivity in the infrared; but since surface temperatures are normalized to those measured by the satellite radiometer, this assumption has little effect. The single cloud layer is taken to be plane-parallel with reflectivity, transmissivity and emissivity characteristic of water spheres with an effective (weighted by cross section) mean radius of 10 μm. Multiple scattering effects are included. The model radiances are, therefore calculated as a function of viewing geometry, cloud top pressure, surface reflectivity and temperature, vertical temperature and humidity distribution, ozone column abundance, and two cloud properties.

[1] Visible channel radiances are expressed as a reflectivity and IR channel radiances are expressed as brightness temperatures.

number of two dimensional clusters which are defined by the following steps. (i) The maximum frequency peak in the IR histogram is identified. (ii) Two half-Gaussian functions are fitted to the peak where the standard deviation on each side is derived by a regression between the radiances and the logarithm of the frequency. (iii) Pixels are assigned to this first cluster according to their distance from the peak radiance: namely, all pixels within one standard deviation, σ, are included in the cluster; all pixels more than 3σ distant are excluded; a number of pixels equal to the extrapolated (Gaussian) frequency (or the total available, whichever is smaller) is included in the cluster for radiances between σ and 3σ distance from the peak radiance. (iv) Using only the pixels assigned to the IR cluster, a VIS histrogram is constructed and Gaussian functions fitted as before. (v) Step (iii) is applied to the VIS histogram, thus defining the first two-dimensional cluster. (vi) All pixels assigned to the first cluster are removed from the histogram. (vii) The steps i–vi are applied to the residual histogram to define a second cluster. If two clusters have overlapping one-σ regions, they are combined into a single cluster. (viii) The procedure is repeated until all of the pixels are assigned to clusters or ten clusters are defined. (ix) If any pixels remain unassigned after ten clusters are defined, they are assigned to the nearest cluster defined by the shortest (two-dimensional) distance between the pixel and the cluster center.

Once all pixels are assigned to clusters and one cluster identified (if possible) as representing the actual surface, the fractional cloud cover, CC, is given by the total number of pixels in all other clusters. In the results presented here, the identification of the actual surface is done by inspection, together with knowledge of the location of the subregion. The cloud and surface properties (RC, TC, RS, TS) are defined by the average radiances over the pixels within σ of the peak frequencies of the appropriate cluster. The resolution of the results is given by the size of the subregion needed for stable statistics; the number of image pixels required is estimated to be $\sim$300.

5) DYNAMIC CLUSTER HISTOGRAM ANALYSIS

This method (Desbois *et al.*, 1982) also analyzes the two-dimensional (one-dimensional at night) frequency histogram of the radiances measured over a geographical subregion in the image; however, both the procedure for assigning pixels to clusters and the interpretation of the measured radiances are different. Unlike the previous method, dynamic cluster analysis isolates two-dimensional clusters defined by the population density in the histogram rather than clusters defined by peaks in two separate one-dimensional histograms. The central concept used to identify clusters is that every surface type in the subregion is represented in the histogram by a compact subdomain of the histogram; i.e., that all points in each subset are close to each other and that subdomains do not overlap. This is equivalent to the assumption that the radiance variation within each surface type or cloud is small compared with the radiance differences between types.

The clusters are identified by the following steps. (i) An initial set of clusters is chosen at random; this selection sets the maximum number [15] of clusters possible. (ii) For each initial cluster, a number of points [30] in the two-dimensional radiance space are selected at random to form the kernel of each cluster. (iii) The center of gravity (i.e., average radiance) and the standard deviation of the kernel point radiances are calculated. (iv) All other pixels in the histogram are assigned to the cluster with the nearest kernel (minimum distance between the pixel and the kernel center of gravity). If any cluster has too few pixels [<50], it is eliminated. (v) The center of gravity and variance of each cluster are calculated using all the pixels in that cluster. (vi) This center of gravity and variance define a new kernel selection. (vii) Steps iii–vi are repeated until the differences between kernel and cluster centers of gravity stop changing.

All pixels are assigned to nonoverlapping clusters (see Desbois *et al.*, 1982, for details). The fractional area covered by each surface type represented by a cluster is given by the number of pixels in that cluster. The actual surface is identified by comparing the radiance values at cluster centers of gravity to specified threshold values. In the results presented here, the surface clusters were determined by inspection of the whole data set. The fractional cloud cover CC is given by the total number of pixels in all clusters other than the surface clusters. The resolution of the results is given by the size of the subregion required for stable statistics; the number of pixels needed is estimated to be >1000.

The identification of histogram clusters was performed both on the 2.5° boxes and on the larger 20° area to compare the statistical effects. Using the larger area allows collection of a sufficient number of pixels for reliable statistics, even with degraded data, and enhances the probability that each cloud type or surface is represented by a sufficient number of pixels. The classification obtained on the larger area is then applied to the smaller subareas; this later approach was preferred in the pilot study results.

4. Cloud detection intercomparison

Since all of the methods considered here determine CC by counting cloudy pixels, intercomparison of CC values is a means of comparing the cloud detection ability of the algorithms. Four different methods of comparing CC distributions for each day and region were employed: differencing, regression, cross-correlation and manual inspection. The first three methods were used to compare results from each algorithm to results from VIS TH at 1 km resolution, to specific

TABLE 2. Correlation of cloud cover distribution over each study region obtained by each algorithm to the distribution averaged over all results. Numbers in the columns are normalized correlation coefficients with the bias in parentheses. Biases are in percent cloud cover.

	VIS TH	IR TH	RT TH	HB TH	AG HIS	DC HIS
Region 1						
DOY 37	0.96 (−3.5)	0.99 (+2.5)	0.98 (+3.1)	0.93 (−3.7)	0.92 (−1.7)	0.93 (+5.4)
DOY 40	0.70 (−0.6)	0.91 (−5.6)	0.63 (+8.5)	0.89 (−5.9)	0.33 (+18.2)	0.88 (−15.4)
DOY 43	0.86 (−1.7)	0.83 (+2.3)	0.93 (+0.4)	0.90 (−4.8)	0.47 (+16.2)	0.84 (−8.7)
DOY 46	0.95 (+7.2)	0.60 (−12.5)	0.92 (+1.2)	0.51 (−5.5)	0.95 (+1.2)	0.96 (+4.9)
DOY 49	0.99 (+3.4)	0.99 (−0.1)	0.99 (−2.5)	0.92 (+2.1)	0.97 (−0.9)	0.98 (−0.9)
Average	0.89 (+1.0)	0.86 (−2.7)	0.89 (+2.1)	0.83 (−3.6)	0.73 (+6.6)	0.92 (−2.9)
Region 2						
DOY 37	0.92 (+3.6)	0.97 (−2.4)	0.98 (+0.7)	0.91 (+10.4)	0.96 (−0.0)	0.98 (−6.2)
DOY 40	0.79 (+7.8)	0.94 (−7.5)	0.94 (+1.7)	0.87 (+7.3)	0.87 (−1.4)	0.97 (−2.7)
DOY 43	0.91 (+2.7)	0.92 (−11.4)	0.96 (+1.1)	0.79 (+4.0)	0.90 (+0.3)	0.89 (+3.1)
DOY 46	0.80 (+8.5)		0.91 (−1.3)	0.80 (+7.8)	0.68 (+4.1)	0.94 (−8.7)
DOY 49			0.89 (+6.9)	0.79 (+9.6)	0.67 (+6.8)	0.83 (−15.3)
Average	0.86 (+5.6)	0.94 (−7.1)	0.94 (+1.8)	0.83 (+7.8)	0.82 (+2.0)	0.92 (−6.0)
Region 3						
DOY 37	1.00 (+0.9)	0.84 (−4.9)	0.98 (+7.9)	0.97 (−5.6)	0.95 (−5.2)	0.99 (+5.6)
DOY 40	0.93 (+0.1)	0.86 (−1.8)	0.96 (+1.6)	0.97 (−0.4)	0.95 (−3.9)	0.90 (+3.3)
DOY 43	0.95 (+1.8)	0.85 (−4.8)	0.98 (+1.7)	0.97 (−1.7)	0.97 (+0.6)	0.98 (+1.9)
DOY 46	0.92 (+2.3)	0.87 (−4.4)	0.94 (−0.5)	0.95 (−1.2)	0.94 (−1.8)	0.97 (+3.8)
DOY 49	0.95 (+2.4)	0.43 (−14.7)	0.97 (+3.3)	0.90 (+3.4)	0.94 (+2.5)	0.98 (+1.2)
Average	0.95 (+1.5)	0.77 (−6.1)	0.97 (+2.8)	0.95 (−1.1)	0.95 (−1.6)	0.96 (+3.2)
Total average	0.90 (+2.7)	0.86 (−5.3)	0.93 (+2.2)	0.87 (+1.0)	0.83 (+2.3)	0.93 (−1.9)

cloud types or situations. Thus, the focus of the discussion in this paper is on these more problematic cases in order to elucidate the workings of the algorithms and to suggest improvements for the ISCCP analysis.

Two classes of problems are discussed: 1) partially cloudy situations where cloudy radiances are not very different from clear sky radiances in one or both of the radiometer spectral channels, and 2) situations where complex variations in the clear sky (surface) properties make their accurate determination difficult. Both of these situations can be considered to be "low contrast" in that the detection signal (the difference between the measured and clear sky radiances) is small compared to the uncertainties in these radiances. Consideration of specific cases in all three regions can be used to separate the effects of the method used to determine clear sky radiances from the effects of the process used to make the cloudy–clear decision.

Figures 3, 4 and 5 display the results of Fig. 2 for pairs of algorithms and also show results by region. In each figure, the results from the two algorithms are displayed as broken lines, while the average over all six methods is shown as a solid line. Figure 3 shows results from VIS TH and IR TH, Fig. 4 shows HB TH and RT TH, and Fig. 5 shows DC HIS and AG HIS. These figures suggest some methodological differences that are further examined below.

The IR TH cloud amount is generally less than the VIS TH value (Fig. 3a), primarily because IR TH misses low-lying clouds over the ocean in Regions 2 and 3 (Figs. 3c and 3d). In Region 1, IR TH obtains larger values of CC because the clear sky radiance used for all five days is the maximum IR radiance observed at each location during the 15-day record. Since a strong storm passed over the region followed by clear, very cold weather, the IR TH method mistakes these cold surface temperatures for cloud. On the other hand, the snow cover produced by this storm causes an overestimate of CC by VIS TH because the 15-day minimum reflectivity is used as the clear sky value for all five days. Overall the largest disagreements between the methods occur over cold, snow-covered land in Region 1 and over oceans in Region 2, where the very low-level clouds are both warm and relatively dark.

Figure 4 shows that, in general, the two bispectral threshold methods agree better than the two single channel methods, probably resulting from the compromises between the VIS and IR threshold decisions. However, Figs. 4c and 4d show that there are some differences between these methods which can be attributed to differences in the precise way that the thresholds are applied. The RT TH method requires that the measured radiances exceed both the VIS and IR thresholds for an image pixel to be classified as cloudy, whereas the HB TH utilizes the IR radiances of all image pixels below a VIS threshold to set an IR threshold. As discussed later, the warm, relatively dark clouds in Region 2 are generally missed by the RT TH

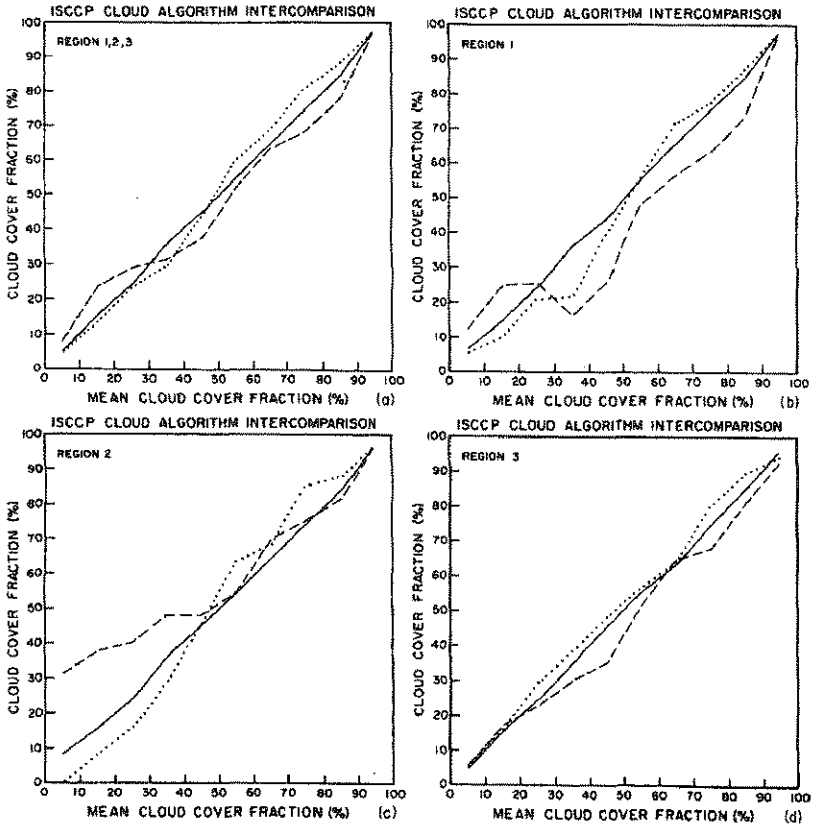

FIG. 4. As in Fig. 3 but showing only results from the HB TH (dashed) and RT TH (dotted) methods.

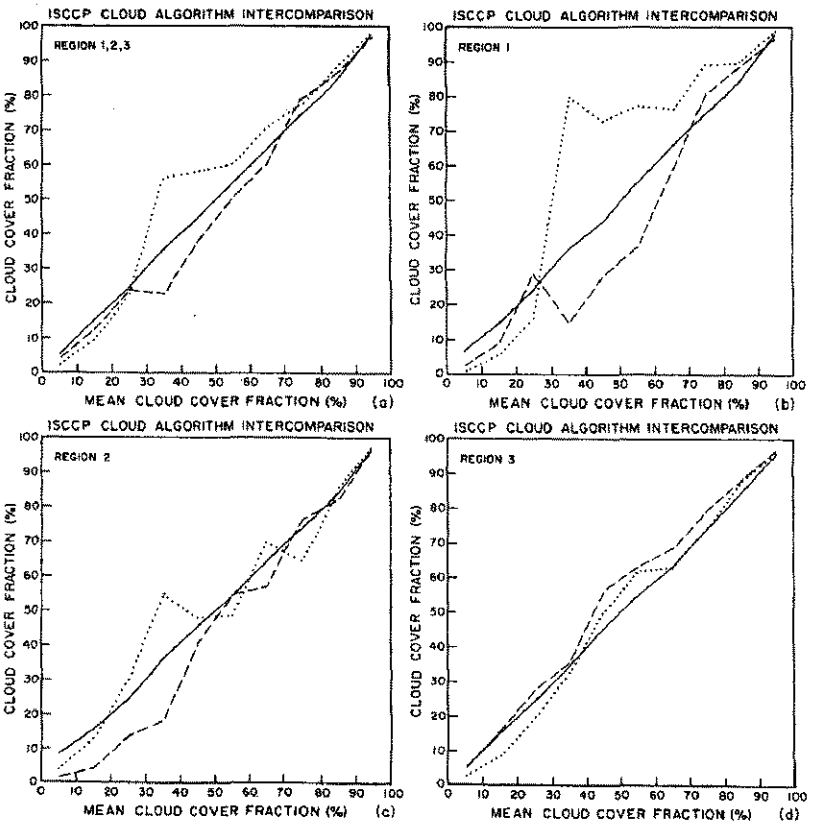

FIG. 5. As in Fig. 3 but showing only results from the DC HIS (dashed) and AG HIS (dotted) methods.

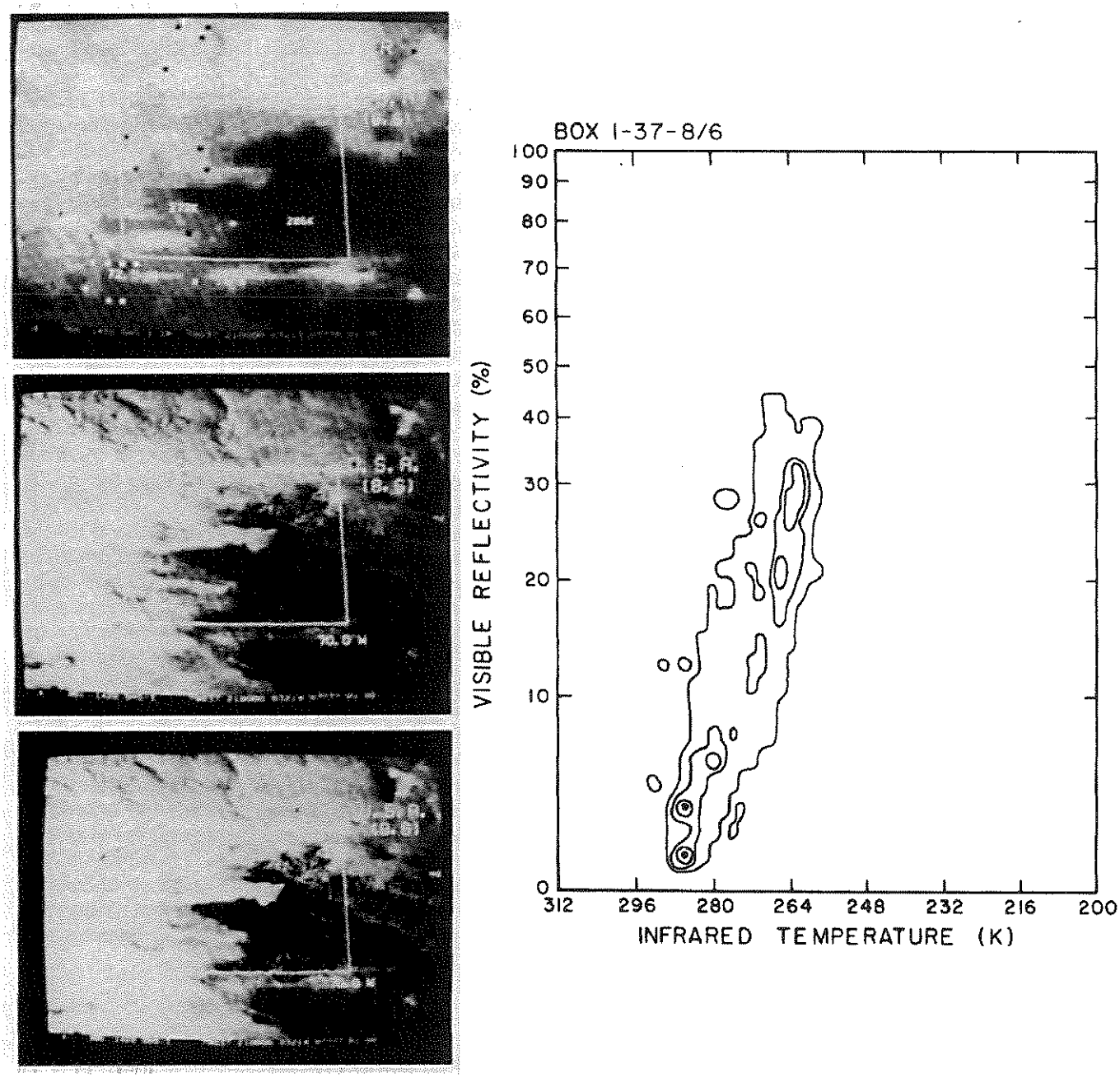

FIG. 6. Data for subregion 1-37-8/6 (see text for numbering convention): (upper photo) IR radiance data showing particular box, (middle photo) VIS image data, (lower photo) VIS image showing only data above VIS threshold. Two-dimensional radiance histogram shows frequency of occurrence of VIS radiances expressed as percent reflectivity (vertical axis) and IR radiances as brightness temperature (horizontal axis). Contours show equal increments in frequency. Results of applying different algorithms shown in Table 3.

method HB TH uses to select its IR threshold produces an apparent overestimate of cloud fraction in the former case, while producing an underestimate in the latter case.

The histograms in Figs. 9 and 10, exhibit small differences in the detailed frequency distribution of the radiances even though the general histogram shapes are similar. These subtle differences, attributable to small changes in cloud properties such as size distribution, lead to changed relationships among the algorithm results. Whereas the RT TH and DC HIS results overestimate cloud fraction (relative to VIS TH) in Fig. 9, these methods underestimate the cloud amount in Fig. 10. All of the methods failed to detect properly a 15% increase in cloud fraction between the two scenes.

Taken together, all of the cases discussed above highlight the interaction between cloud properties, especially for broken clouds, and the methodology used to separate clear and cloudy pixels; that is, all of the

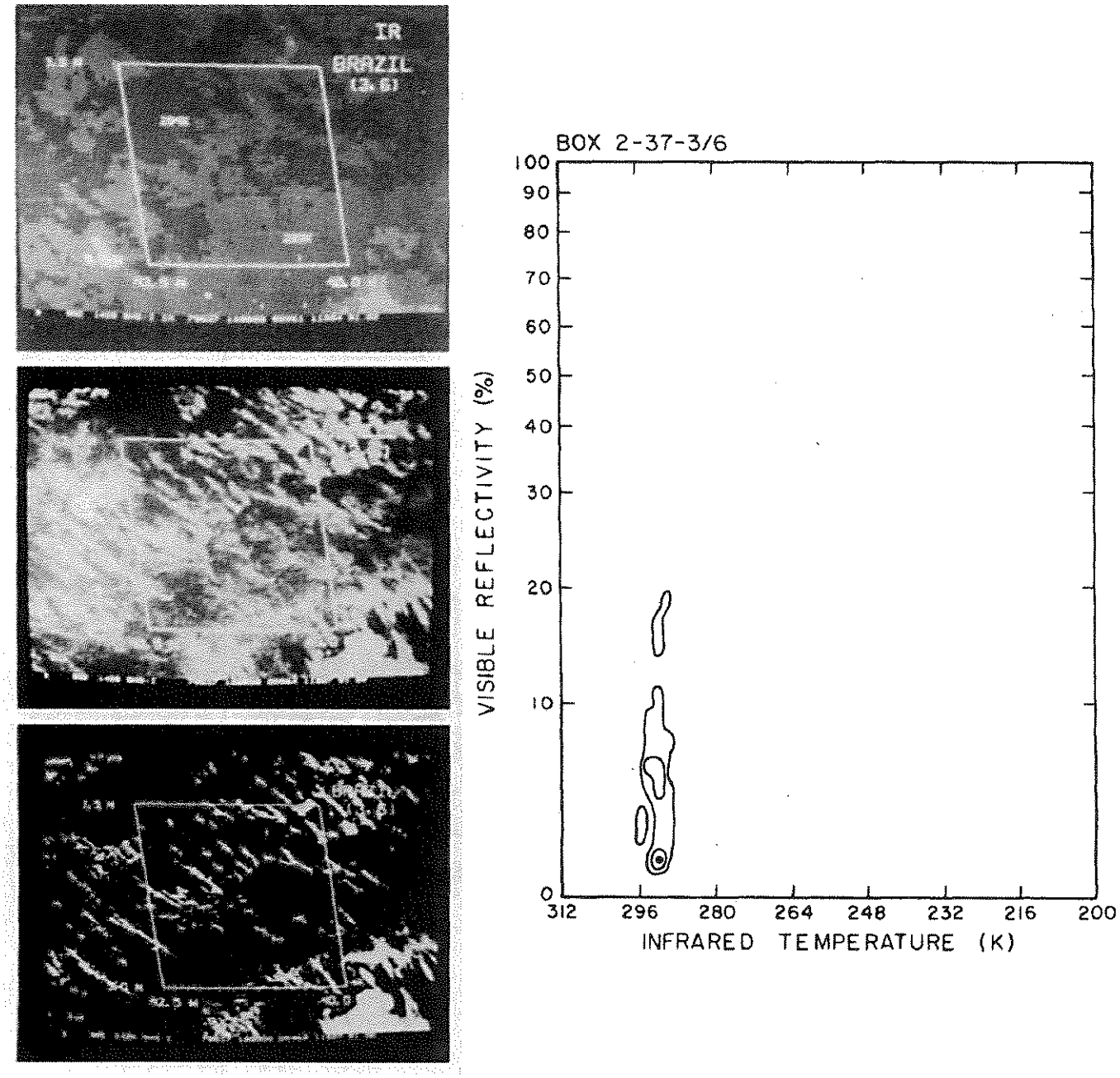

FIG. 8. Data for subregion 2-37-3/6 (see caption to Fig. 6). Note that IR contrast shown in upper photo is only 1 K.

clear-sky radiances produce two distinct clusters. Where the cloud forms another distinct cluster in the histogram (Fig. 11a), DC HIS and AG HIS not only agree with each other on the value of CC, but also agree well with the threshold methods. On the other hand, more broken cloudiness leads to a more complex histogram (Fig. 11b). This situation produces disagreement between the histogram methods and the HB TH method. (In this same scene, some of the thinner, low-lying cloud over ocean is missed by the RT TH method, whereas the IR TH method confuses some of the cooler mountains for cloud.)

An even more confusing case is illustrated in Fig. 12 for a region near the Great Lakes with partial ice cover and snow covered fields and forests. In this case the darkest area is also the coldest, representing clear skies over snow-covered forests in Canada. Because of a rapidly developing cyclone storm to the south, moving towards the east coast, the area is partially covered by cirrus/stratus which remains in a relatively constant location over a few days. Completing the confusion in this scene is the strong surface temperature gradient associated with the cloud front making the clear-sky temperature very similar to the apparent cloud top

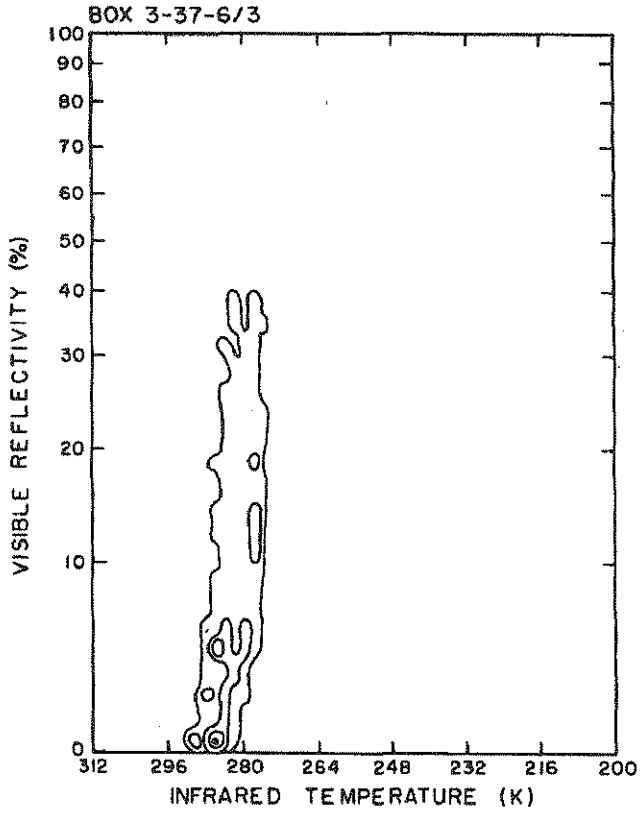

FIG. 10. Radiance histogram for subregion 3-37-6/3 (see caption to Fig. 6).

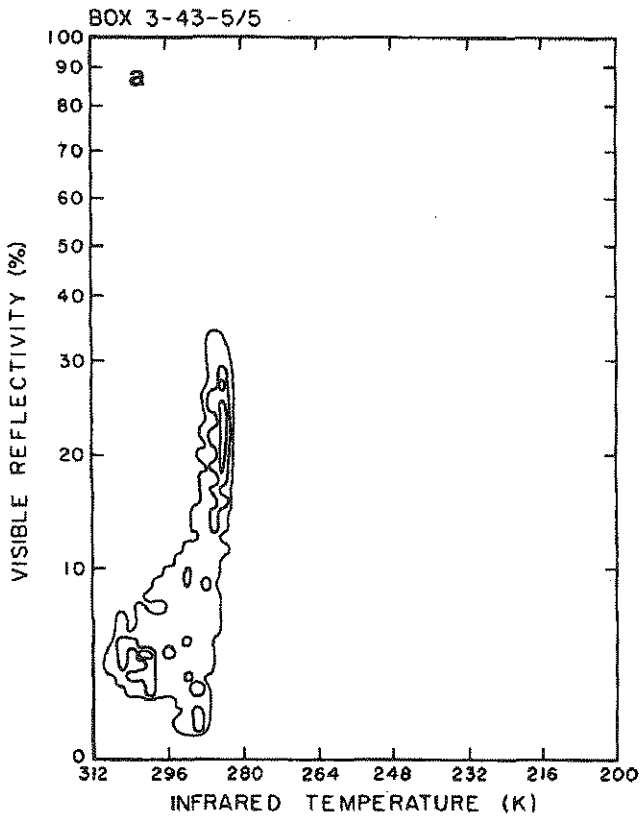

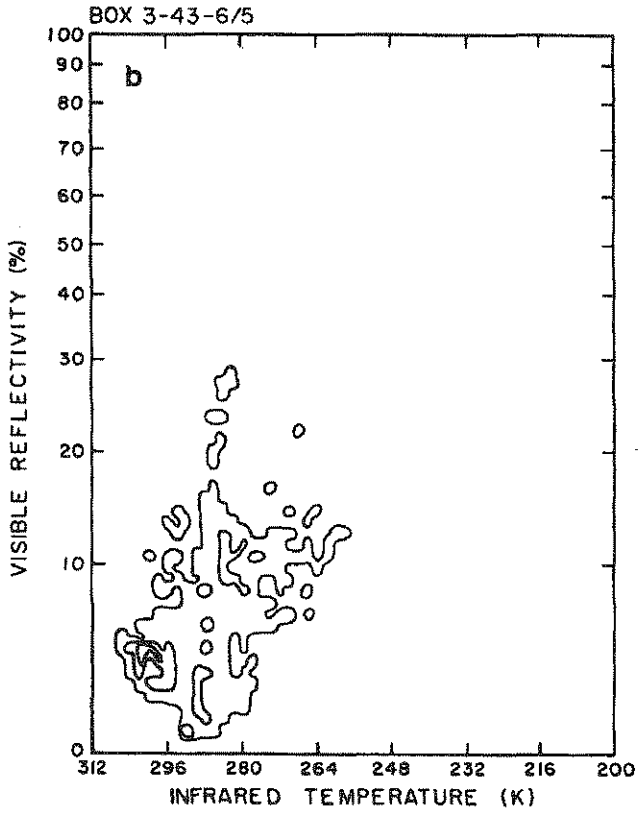

FIG. 11. Radiance histograms for subregion (a) 3-43-5/5 and (b) 3-43-6/5.

main relatively constant in time, then such an analysis can provide the detailed, pixel-by-pixel distribution of RS and TS. With this information the threshold methods can treat image pixels individually and are better able to handle these complex cases. A recent test of this time compositing approach with a histogram method shows that its results are also improved when the complicated surface clusters can be described (Desbois and Seze, 1984). In principle, then, all cloud algorithms can handle spatially complex scenes if accurate determinations of RS and TS are available and this information is utilized in the analysis.

c. Time varying background

The last case discussed above actually represents one of the most difficult classes of partially cloudy scenes to analyze correctly, since the surface properties are not only spatially complex but also varying rapidly in time. Although the use of clear sky values derived from satellite time composites can, in principle, account for the spatial variations of RS and TS, time variations in these quantities preclude a simple statistical analysis to obtain these values. A typical situation involves a rapidly developing winter cyclone. In only 24 h, surface temperatures in regions which began the period ahead of a cold front, fall by 5–10°C with passage of the front;

v) A second difficulty with identification of cirrus and boundary layer cumulus for current cluster analysis schemes is that these two cloud types do not always form a distinct cluster in the radiance histogram (see examples in World Climate Program, 1984). Threshold techniques, working with individual image pixels are not affected by this property. Nevertheless, the distinctive histograms produced by these clouds (see discussion in Section 5) do indicate potential additional information that can only be obtained by statistical methods. General techniques to recognize such patterns are not yet available, however.

vi) Detection of the difficult cloud types by a bispectral threshold technique is not completely straightforward. If clear-sky VIS and IR radiances are accurately known, the proper method would be to classify as cloud any image pixel which passes *either* threshold test. Neither RT TH or HB TH used this approach. Instead RT TH required a pixel to pass *both* threshold tests; but, since the IR test came first, RT TH results depend more on the IR test and they resemble IR TH more. Analysis method HB TH derives an IR threshold value, which is influenced by any clouds which fail a VIS threshold test, in order to obtain a better estimate of CC. However, as discussed in the specific case of boundary layer cloud, use of an IR threshold, however calculated, seems inappropriate.

vii) These conclusions are equivalent to saying that we have more experience with threshold methods than the newer statistical methods but that much improvement of threshold methods is still possible. The workshop participants selected a threshold method for the ISCCP algorithm, but did not choose any of the particular algorithms tested in this study. Rather, a new algorithm was designed (see Section 6) to overcome some of the deficiencies revealed by the intercomparison study.

5. Cloud analysis

After separating cloudy and clear scene radiances, further quantitative analysis of the cloudy sky radiances is required to meet the scientific objectives of ISCCP (Table 1, World Climate Program, 1982b). The large data volume produced by the high resolution radiometers on operational satellites requires compression by at least a factor of 1000 to make this analysis practicable, yet the effect of partially covered FOVs on determination of fractional cloud cover urges use of maximum resolution observations. Algorithm tests were directed towards study of some data compression schemes and of some techniques to account for partially covered FOVs.

a. Data compression

Since most operational radiometers produce much higher resolution visible channel data than IR channel data, consideration of data compression involves both the relation between the two channels and overall reduction of data volume. ISCCP objectives call for retrieval of those cloud properties which affect Earth's radiation budget; therefore, regardless of the way that partially covered FOVs are handled, the basic data for quantitative analysis of cloud optical properties are spectral radiance measurements of identical scenes. Since the ratio of VIS to IR resolution is very different for the available radiometers, no consistent method of utilizing the higher visible resolution has been developed. Hence, the first step in data compression is averaging of visible radiance measurements to produce a visible image pixel matched to the lower resolution IR image pixel.

Further data compression can be obtained by more degradation of spatial resolution either by averaging or sampling. (A few more sophisticated compression schemes were discussed by the workshop participants, but no proposals for recovering higher resolution cloud results from such methods were available.) The pilot dataset was used to examine whether spatial averaging or sampling should be used to produce the additional data volume reduction. Each algorithm group repeated some of their analyses with radiance data averaged to 32 km resolution and sampled to 32 km spacing. All methods exhibited the same behavior: CC calculated by counting cloudy pixels systematically increased by 5–10% when the data are averaged (cf., Shenk and Salomonson, 1972), whereas average results with sampled data were almost identical to the full resolution results. These test results recommend that further data compression by spatial sampling is the best strategy for climatological data sets.

b. Analysis of cloud cover

All of the cloud algorithms discussed thus far determine fractional cloud cover by counting all pixels classified as cloudy. If clear-sky radiance values are accurately known, then all algorithms can be tuned to detect all image pixels containing any amount of cloud; however, for broken clouds with individual cloud elements smaller than the radiometer FOV, this approach leads to an overestimate of fractional cloud cover. Both threshold and statistical methods can also be tuned to classify cloudy pixels, with lower partial coverage of the FOV, as clear to compensate for this effect; but, as the results in Section 4 show, not only is the required tuning dependent on the cloud types and size distribution, but also such tuning can cause the algorithm to miss certain cloud types altogether. The climatological importance of these difficult cloud types requires the ISCCP algorithm to detect their presence, but the problem of what cloud fraction to assign remains.

Some of the case studies discussed in Section 4 were designed to test whether any of the statistical methods

TH), all applied to 4-km resolution AVHRR data, show that cloud amounts are generally reduced and suggest some agreement between the two methods (see World Climate Program, 1984).

Several issues remain to be explored, however. All of the methods discussed in this section attempt to improve fractional cloud cover determinations using some statistical property of the radiance spatial distribution; however, they also assume some constant radiative property and, more critically, assume that some particular radiance value represents a completely cloud covered image pixel. Broken cumulus clouds, for which the FOV problem is most severe, do not always oblige by providing *any* completely cloud covered pixels. Figure 13 illustrates the fundamental dilemma by showing the interrelation between cloud fraction, optical thickness, and top temperature for two cases: many possible solutions can explain one VIS and IR radiance observation. Unique identification of which variables are responsible for the variation in the observed radiances may depend on the correct identification of different cloud types and is not currently possible on a global basis. Much more study of these and other suggestions for treating partially covered FOVs is required.

c. Analysis of diurnal variations

The main focus of the pilot study was on the analysis of cloud amount using both VIS and IR radiance measurements. However, the goal is to design an algorithm which obtains the complete diurnal variation of clouds. For nighttime observations, this requires the algorithm to be applied to IR radiance data, alone, for global results. This produces two difficulties for analysis of the diurnal variation of clouds. First, all algorithms become, to some degree, less capable of detecting low-lying clouds, particularly over land where the surface temperature (and clear-sky IR radiance) is generally closer to the cloud top value and undergoes rapid and spatially complex variations (see discussion in Minnis and Harrison, 1984a,b). If the surface reflectivity is known, VIS radiance measurements during the day allow for a more sensitive detection of low clouds. As a consequence, proper evaluation of the diurnal variation of *low* cloud cover is difficult. Second, with only IR information available, the quantitative analysis of cloud optical properties is constrained in a different fashion. Optically thin clouds, in particular, cannot be uniquely distinguished from warmer, optically thick clouds; thus, the diurnal variation of cirrus may not be reliably measured.

6. ISCCP cloud algorithm design

Figure 14 illustrates the ISCCP operational algorithm, which has four major components: 1) derivation of clear-sky radiance maps from satellite radiance and correlative data that correspond to each image, 2) application of radiance thresholds, 3) comparison of cloudy radiances to the cloud model radiances, and 4) histogram and diagnostic analysis of radiances and

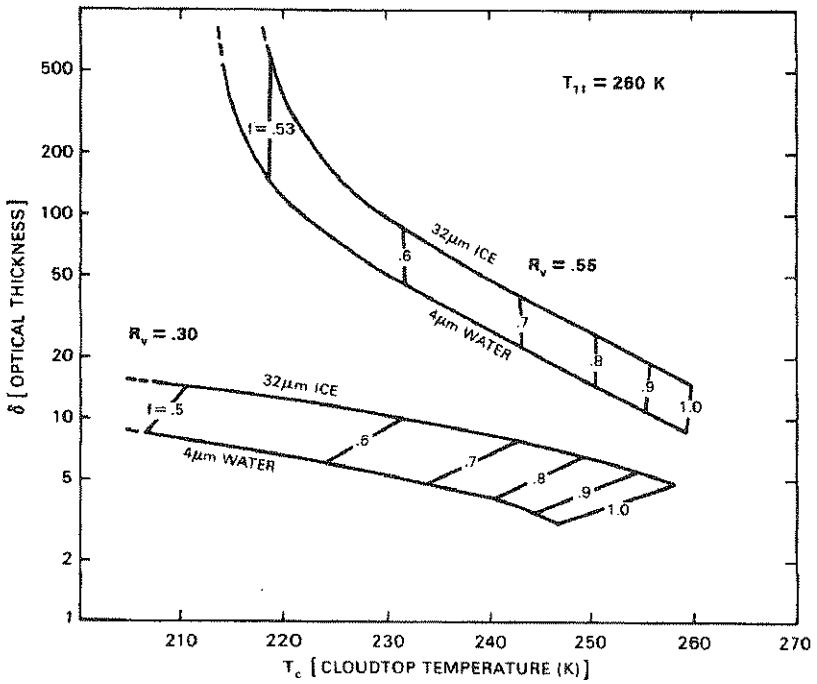

FIG. 13. Variation of VIS and IR radiances for cloud with fixed properties but covering variable fractions of the satellite radiometer FOV (from Arking).

thus, correlative data from other sources are used primarily to fill gaps in satellite observations of clear-sky radiances or to resolve ambiguous situations. The three basic steps in the analysis, which were suggested by the algorithms in the pilot study are: classification of satellite images, compositing satellite images, and filling and interpolation using correlative data.

Each of these steps focuses on a different aspect of the complete clear-sky radiance distribution because the space–time variations differ between spectral channels and vary with surface type. Clear-sky IR radiances over the ocean are relatively constant in time and less variable in space compared to those over land. Clear sky VIS radiances are much more constant in time but more variable in space than clear-sky IR radiances. The behavior of both land and ocean is altered at high latitudes by the presence of snow and sea ice. Thus the clear sky radiance analysis differs somewhat over each of four surface types: land, snow/ice-covered land, ocean and ice-covered ocean.

The first step is classification of the satellite IR images into cloudy and "clear" categories based on the characteristic of the spatial distribution of radiances that, within many subregions approximately 100–200 km square, some clear sky is present and the cloud top temperature is very different from clear sky. Thus any pixels found to be much colder than the warmest pixel in that subregion are labeled cloudy. In general, this crude threshold properly identifies most high and middle level clouds constituting about one-third of the image and about half of the total cloud; however, in some areas with low cloud or in some regions completely covered by layered clouds, no pixels are classified as cloudy. Next each pixel is classified by the time variation of the IR radiance: any pixel that is much colder than on the previous day or the following day is labeled as cloudy. This step works for many clouds that have top temperatures much colder than clear sky and move or develop significantly in one day. Again, most middle and high clouds associated with synoptic or mesoscale storm systems, as well as some broken cumulus clouds, are detected. About one-third of the image is classified as cloudy by this step, but much of this cloud was also identified in the first step. The total detected by either step is a little more than half of the total cloud present; the total detected by both steps together is about two-thirds of the total cloud. Image classification thus serves to identify the "obvious" clouds in IR radiance images.

The second step, compositing, examines the time and space variations of radiances in a different way. The cluster analysis methods (Desbois *et al.*, 1982; Simmer *et al.*, 1982) and the method of Coakley and Bretherton (1982) all make use of the general observation that clear regions exhibit smaller spatial variations in IR radiance than do broken cloud regions. However, some low cloud types, particularly the marine stratocumulus studied by Coakley and Bretherton, can also exhibit small spatial variance when cloud cover is complete. Trade-wind cumulus at very low levels can also exhibit small spatial variances even though cloud cover is much less than complete. Over ocean, where time variations of both VIS and IR clear sky radiances are small, some cloudy radiances confused with clear in the first step can be recognized by their variation in time, as suggested by Minnis and Harrison (1984a) and Rossow *et al.* (1985). Thus the frequency of occurrence of the radiance values associated with clear sky is generally higher when a small spatial domain is examined over time. The extremum of the radiance distribution, usually associated with clear sky (minimum reflectance, maximum brightness temperature), is too sensitive to unusual circumstances, but should generally be close in value to the average over a small space and time domain if that region is clear of clouds. The compositing step checks for this condition using only the radiance values classified as "clear" by the first algorithm step. The results of this step can reinforce or contradict that of the first step, especially over land where clear sky IR can vary rapidly in time. Contradictions are labeled as "confused."

Statistical studies of the spatial (Rossow *et al.*, 1985) and temporal (Minnis and Harrison, 1984a) correlations of clear-sky IR radiances suggest that some (limited and cautious) interpolation can be done to obtain more coverage of their distribution. In particular, IR radiances in confused subregions which are similar to radiances in adjacent clear subregions provide a clue to the proper value in that location.

At this stage, there are some locations or times for which clear-sky radiances have not been obtained because of persistent cloud cover, rapidly varying (i.e., confusing) surface properties or ambiguities in the previous analysis steps. The third step in the analysis is to compare the incomplete clear sky measurements obtained from the satellites with colocated conventional observations. This comparison (by region) is used to provide a statistical relationship used to translate the correlative data into clear sky radiances as measured by the satellite (see Rossow *et al.*, 1985) and to fill any gaps in the satellite analysis. The advantage of this approach is that radiometer calibration effects and radiative model deficiencies are nearly eliminated by removing any bias between satellite and correlative data. Furthermore, these values are generally only used in regions which are mostly cloudy and, therefore, do not affect the detection step very strongly.

b. Threshold application

The data in a particular image are now compared to the clear sky values modified by a threshold amount, ΔR and ΔT. These threshold amounts are meant to account for three distinct effects. The first is the effect on the analysis of measurement and processing errors

Program, 1984), the structure of the radiance histogram seems diagnostic of different cloud morphologies. Results of an experimental classification scheme will be reported.

Several types of quality labels will be reported with the results to document the choices made by the analysis program, to evaluate the consistency of the results, and to warn of difficult situations which give less reliable values. In the latter category are retrievals performed under temperature inversion conditions, over snow or ice covered surfaces (especially for geometries which cause thinner clouds to be darker than the surface) and in sun glint geometries. These quality labels allow for later consistency checks to verify that the less reliable retrievals do not introduce any bias in the results.

e. Reported variables

Although the analysis map grid used for the diagnostics is an equal area map, necessary to preserve proper statistical uniformity over the globe, tests have shown that remapping of such results to other projections does not affect the statistical properties of the results (Rossow and Garder, 1984). Thus, ISCCP cloud data can be easily remapped to other commonly used grids, such as the square latitude–longitude format. The spatial resolution of the results is equivalent to 2.5° near the equator. Results will be presented for every 3 h over the whole globe and averaged over calendar months. The variables reported for each grid box are the fractional cloud cover and error estimate and the mean and variance of cloud optical thickness, top temperature and top pressure for (at least) six cloud types: total, low, middle, high, cirrus and deep convective. Each of these types is defined by cloud top pressure and/or optical thickness as follows: low cloud top pressure, PT $\geqslant$ 700 mb; middle cloud top pressure, 700 $>$ PT $\geqslant$ 500 mb; high cloud top pressure, 500 mb $>$ PT. The pressure levels correspond roughly to 3 and 6 km altitudes. Cirrus and deep convective clouds are defined (during the day) to be high clouds with optical thickness, $\tau \leqslant 6$ and $\tau > 32$. The former definition is selected to insure that the clouds identified as cirrus have properties which lead to positive radiative feedback on climate. Higher clouds could be somewhat thicker and still provide a small positive feedback.

Also reported are the mean and variance of total and clear-sky radiances (for all available spectral channels), surface temperature, humidity and visible reflectivity, surface type and topography, atmospheric temperature and humidity profiles, and ozone column abundance. Additional information about the amount and kind of data used in the analysis and the quality labels are also included. On a somewhat larger regional scale, the histogram and other spatial distribution diagnostics, plus surface and cloud type classifications, are reported. Monthly averages of these results will include a mean diurnal cycle and other time distribution diagnostics.

f. Recommendations for future research

The research component of ISCCP is concerned with validation of the cloud climatology produced by the algorithm described above; however, validation has two different, but related, objectives. The first is to clarify the interpretation of the climatology dataset so that it can be used to study cloud behavior and to improve the treatment of clouds in climate models. The focus of this type of study is on understanding the atmosphere and how to model it. The second objective is to confirm the cloud parameterization used in the analysis of satellite data and to improve analysis techniques. Progress towards both of these objectives requires improved understanding of the interaction of radiation and clouds. The recommendations from the Workshop participants concern the second objective.

Future work to improve cloud algorithms should focus on four areas: development of histogram and other statistical methods, development of multichannel radiative transfer methods, study of cloud morphology statistics, and investigation of methods to infer additional cloud properties from satellite observations. Several statistical approaches have been proposed to obtain better cloud cover values than possible with pixel counting; however, the pilot study results suggest that these methods may work only when the clouds behave as assumed in the technique. Proper exploitation of these methods may require identification of cloud or scene type before application to account for the different statistical behavior that seems related to different cloud types. If further study of cloud property spatial statistics shows a recognizable pattern for each cloud morphological type, then these methods may be used both to classify cloud types and to calculate more accurate cloud cover.

Another way to resolve the dilemma of recognizing the difference between radiance changes due to cloud cover variations and those due to optical property variations is to employ at least one more independent radiance measurement to retrieve a unique set of cloud parameters. Several existing radiometers have other spectral channels which could be tested for this purpose. Whether pixel-by-pixel retrievals or histogram methods are to be employed probably depends on the spectral channels used; both types of multichannel techniques should be tried. All available spectral channels are saved as part of the ISCCP radiance dataset.

The structures exhibited by the histograms are, at least in part, an expression of the fact that clouds or cloud fields are generally large-scale features controlled

for cloud parameter determination. *Mon. Wea. Rev.*, **105**, 446–457.

Rossow, W. B., (Ed.), 1981: Clouds in climate: Modeling and satellite observational studies. *Workshop Rep. NASA Goddard Institute for Space Studies*, 222 pp.

——, and L. Garder, 1984: Selection of a map grid for data analysis and archival. *J. Climate Appl. Meteor.*, **23**, 1253–1257.

Saunders, R. W., 1985: Monthly mean cloudiness observed from METEOSAT-2. *J. Climate Appl. Meteor.*, **24**, 114–127.

Schiffer, R. A., and W. B. Rossow, 1983: The International Satellite Cloud Climatology Project (ISCCP): The first project of the World Climate Research Programme. *Bull. Amer. Meteor. Soc.*, **64**, 779–784.

Shenk, W. F., and V. V. Salomonson, 1972: A simulation study exploring the effects of sensor spatial resolution on estimates of cloud cover from satellites. *J. Appl. Meteor.*, **12**, 214–220.

Simmer, C., E. Raschke and E. Ruprecht, 1982: A method for determination of cloud properties from two-dimensional histograms. *Ann. Meteor.*, **18**, 130–132.

Wielicki, B. A., and J. A. Coakley, 1981: Cloud retrieval using infrared sounder data: Error analysis. *J. Appl. Meteor.*, **20**, 157–169.

World Climate Program, 1982a: Report of the planning meeting on International Satellite Cloud Climatology Project (ISCCP), Geneva, August 1982, WCP-28.

——, 1982b: The International Satellite Cloud Climatology Project (ISCCP) Preliminary Implementation plan (Rev. 1), WCP-35.

——, 1983a: Report of the First Session of the International Working Group on Data Management for the International Satellite Cloud Climatology Project (ISCCP), New York, December 1982, WCP-42.

——, 1983b: Report of the Second Session of the International Working Group on Data Management for the International Satellite Cloud Climatology Project (ISCCP), New York, April 1983, WCP-52.

——, 1984: The International Satellite Cloud Climatology Project (ISCCP): Cloud analysis algorithm intercomparison. March 1984, WCP-73, pp. 74.

Comparison of ISCCP and Other Cloud Amounts

WILLIAM B. ROSSOW

NASA Goddard Institute for Space Studies, New York, New York

ALISON W. WALKER

Hughes STX, New York, New York

LEONID C. GARDER

Columbia University, New York, New York

(Manuscript received 10 June 1992, in final form 12 May 1993)

ABSTRACT

A new 8-year global cloud climatology has been produced by the International Satellite Cloud Climatology Project (ISCCP) that provides information every 3 h at 280-km spatial resolution covering the period from July 1983 through June 1991. If cloud detection errors and differences in area sampling are neglected, individual ISCCP cloud amounts agree with individual surface observations to within 15% rms with biases of only a few percent. When measurements of small-scale, broken clouds are isolated in the comparison, the rms differences between satellite and surface cloud amounts are about 25%, similar to the rms difference between ISCCP and Landsat determinations of cloud amount. For broken clouds, the average ISCCP cloud amounts are about 5% smaller than estimated by surface observers (difference between earth cover and sky cover), but about 5% larger than estimated from very high spatial resolution satellite observations (overestimate due to low spatial resolution offset by underestimate due to finite radiance thresholds). Detection errors, caused by errors in the ISCCP clear-sky radiances or incorrect radiance threshold magnitudes, are the dominant source of error in monthly average cloud amounts. The ISCCP cloud amounts appear to be too low over land by about 10%, somewhat less in summer and somewhat more in winter, and about right (maybe slightly low) over oceans. In polar regions, ISCCP cloud amounts are probably too low by about 15%–25% in summer and 5%–10% in winter. Comparison of the ISCCP climatology to three other cloud climatologies shows excellent agreement in the geographic distribution and seasonal variation of cloud amounts; there is little agreement about day/night contrasts in cloud amount. Notable results from ISCCP are that the global annual mean cloud amount is about 63%, being about 23% higher over oceans than over land, that it varies by <1% rms from month to month, and that it has varied by about 4% on a time scale ≈2–4 years. The magnitude of interannual variations of local (280-km scale) monthly mean cloud amounts is about 7%–9%. Longitudinal contrasts in cloud amount are just as large as latitudinal contrasts. The largest seasonal variation of cloud amount occurs in the tropics, being larger in summer than in winter; the seasonal variation in middle latitudes has the opposite phase. Polar regions may have little seasonal variability in cloud amount. The ISCCP results show slightly more nighttime than daytime cloud amount over oceans and more daytime than nighttime cloud amount over land.

1. Introduction

The International Satellite Cloud Climatology Project (ISCCP) was established in 1982 as the first project of the World Climate Research Programme (WCRP) to collect and analyze a globally uniform satellite radiance dataset to produce a new cloud climatology (Schiffer and Rossow 1983). The basic dataset that is analyzed is a sampled and calibrated version of visible (VIS $\approx 0.65 \pm 0.15$-μm wavelength) and "window" infrared (IR $\approx 11 \pm 1$ μm) imagery from an international suite of weather satellites, both geostationary and polar orbiting, called the stage B3 dataset (Schiffer and Rossow 1985). The first step in the analysis, called cloud detection (Rossow 1989), separates the satellite observations (image pixels) into clear and cloudy categories. Key objectives are to understand the meaning of "clear" and "cloudy" and the significance of variations of the number of locations that are cloudy, commonly referred to as variations of cloud amount.

In two companion papers (Rossow and Garder 1993a,b), the design of the cloud detection method is fully described, supporting analyses of radiance statistics are presented, and the methodology is validated by verification of the inferred clear radiances. This paper assesses the accuracy of the ISCCP cloud amounts by quantitative comparisons to other, higher spatial

Corresponding author address: William B. Rossow, NASA Goddard Institute of Space Studies, 2880 Broadway, New York, NY 10025.

with the effects of sunlight on the difference between air and solid surface temperatures. After removing the monthly mean diurnal cycle from both datasets to isolate the synoptic (day to day) variations, the rms differences are about 4 K, somewhat larger in winter than in summer. Since the estimated error in clear IR radiances is significantly smaller than the assumed IR radiance threshold value of 6 K, ISCCP cloud amounts are underestimated by 3%–6% over land. There is evidence for more cloud contamination of the clear IR radiances over higher-latitude land areas, especially in winter, with a consequent negative bias of cloud amount of 6%–10%.

The surface reflectance of open water is generally very low, but it varies strongly with illumination and viewing geometry. The estimated uncertainty in the inferred clear VIS radiances appears to be consistent with the assumed threshold value of 3%; but since the VIS threshold is a radiance difference, rather than a reflectance difference, the ISCCP algorithm is actually too conservative at larger solar zenith angles. The VIS radiance test is not used for near-glint geometries because errors are >20% rms. There are no available global surveys of land VIS reflectances to compare with the ISCCP values; however, direct comparisons of ISCCP values from different years and seasons show differences that are 3%–5%, rms, slightly smaller than the assumed VIS radiance threshold value of 6%.

The temperatures and reflectances for surfaces covered by snow and sea ice are examined separately because proper separation of clear and cloudy situations is expected to be much more difficult. Climatologies of sea ice surface temperatures indicate good agreement with ISCCP values except possibly in winter, where the ISCCP values might be biased high by ~2 K; ISCCP surface temperatures on the high ice sheets (Greenland and Antarctica) are generally consistent with published climatologies. Uncertainties in temperatures for ice- and snow-covered surfaces appear consistent with the assumed IR radiance threshold value of 4 K. ISCCP sea ice reflectances also agree within 10% of published estimates for the Arctic. However, since the ISCCP VIS threshold was set at 12% radiance difference, which is equivalent to a reflectance difference >20% for typical solar zenith angle values, the VIS threshold test was effectively eliminated over snow and ice surfaces. As a consequence about 3%–5% of low-level cloud, especially over sea ice, was missed.

The purpose of this paper is to compare ISCCP cloud amounts with other measurements of similar quantities to assess sources of error that arise when converting a detection result (spatial frequency of occurrence) to a fractional coverage of area. Comparison to several different types of measurements also provides an overall estimate of the uncertainties of the ISCCP cloud amounts. We focus most of our attention on surface weather observer estimates of sky cover because they differ most from the satellite measurements. Surface observers view clouds from below rather than from above, which affects their relative sensitivity to the presence of clouds: ground-based observers are probably better able to detect very low-level, highly broken clouds than satellites, but they are probably less able to detect high, thin cirrus than satellites. Since ground observers use a "visible radiometer" (their eyes), their ability to detect cloudiness at night is less reliable (Hahn et al. 1993). Surface observations have higher spatial resolution than most satellites, varying between about 1 m overhead to 10 m at 30-km range (Allen 1973), and cover an effective area of about 3000 km^2 [radius about 30 km, Barrett and Grant (1979), Henderson-Sellers et al. (1987)]. However, since sky cover is reported in octas (12.5%), the effective spatial resolution is much lower.

Section 2 describes the ISCCP cloud datasets and the other datasets used in this study. Section 3 presents comparisons between ISCCP and individual surface observations and discusses errors in interpreting ISCCP cloud amounts as fractional areal coverage. Section 4 compares the ISCCP cloud amount climatology with the surface observation climatology and two other satellite climatologies. Section 5 summarizes estimates of uncertainties in ISCCP cloud amounts and notable features of earth's cloud cover described by the ISCCP climatology.

2. Data

a. ISCCP cloud amount

The IR and VIS radiances [stage B3 data, Schiffer and Rossow (1985)] analyzed by ISCCP are samples of the original weather satellite images at 3-h and 30-km intervals (polar orbiter data are not sampled in time). The individual samples (pixels) represent the original IR fields of view (FOV) with sizes ranging from 4 to 7 km (areas of about 10 to 150 km^2). The presence or absence of cloud is decided for every individual sample: cloud amount for a single pixel is either 0% or 100%. During daytime[1] two cloud detection results are reported, one based on threshold tests of both VIS and IR radiances (called the VIS/IR cloud amount) and one based solely on the IR threshold test (called IR cloud amount) that is equivalent to the result reported during nighttime.

Statistics from the analysis of individual pixels are reported in two datasets, stage C1 and C2, in an equal-area map grid equivalent to 2.5° at the equator (Rossow and Schiffer 1991; Rossow et al. 1991). Each grid cell (area of 77 000 km^2) contains from 20 to 120 pixels at one time; thus, the ISCCP spatial sampling is equivalent to sampling 5% to 15% of the area at each time. Cloud amounts in grid cells are determined for the

[1] Daytime is defined by solar zenith angles <78.5°.

as SOBS. We use monthly mean total cloud cover maps that are compiled separately for land and ocean. For the day/night contrast comparisons we use seasonal means compiled separately at 8 synoptic hours for land and ocean. We use only data from 1971 to 1981 where both land and ocean are available. All data are remapped to an equal-area map grid equivalent to 5° lat by 10° long at the equator for comparison with the other cloud climatologies.

c. *Nimbus-7 cloud climatology*

Radiance measurements made twice daily (near noon and midnight) at an infrared (11.5 μm) wavelength and near noon at an UV (0.37 μm) wavelength from the *Nimbus-7* satellite have been analyzed to obtain a global cloud-cover climatology covering the period April 1979 to March 1985 (Stowe et al. 1988, 1989). We use the complete years 1980–1984 and refer to this dataset as *Nimbus-7*. Monthly mean total cloud cover fractions are compiled in an equal-area map grid with a resolution of about 500 km (equivalent to about 4.5° at the equator). Cloud amounts are determined in three steps: 1) counting the fraction of observations where the infrared radiance is lower by some threshold amount than a clear-sky value at each location, date, and time of day, where the clear IR value is determined from the U.S. Air Force analysis of surface air temperature measurements from weather stations, 2) calculating the ratio of observed UV reflectance to a model of reflectance as a linear function of cloud amount, and 3) combining the IR and UV cloud amounts (Stowe et al. 1988). We refer to the first set as the IR results and the third set as the IR/UV results. All data are remapped to an equal-area map grid equivalent to 5° lat by 10° long at the equator for comparison with the other cloud climatologies.

d. *METEOR cloud climatology*

A global, long-term climatology of monthly mean total cloud amount covering the years 1966 to 1988 has been produced from the manual analysis of imaging data from several satellites by different methods and can be obtained from the Hydrometeorological Center, Moscow, the National Meteorological Center (NMC) Climate Analysis Center, Washington D.C., or from the NASA Climate Data Center, Greenbelt, Maryland [see Mokhov and Schlesinger (1993) for details]. In order to avoid the effects of changed analysis methods and sparse sampling, we use only the results for the period from 1976 to 1988. These are obtained by the same interpretation of infrared (8–12 μm) images (and some visible images) from the METEOR series of weather satellites and are mapped at 5° × 10° resolution. For comparison to the other cloud climatologies all data are remapped to an equal-area grid equivalent to 5° lat by 10° long at the equator and gaps in the data are filled using linear interpolation over time.

3. Comparisons to higher-resolution datasets

a. *Comparison to individual surface observations*

All available ind-SOBS data for three months (January 1984, July 1985, October 1986) were matched to individual ISCCP results for the same locations, dates, and times of day (over 670 000 cases). Figure 1 shows the distribution of differences between the ISCCP and ind-SOBS cloud amounts aggregated over all three months; Table 2 summarizes the results for each month as well. On average, the ISCCP results are lower than the ind-SOBS results by about 11% with a standard deviation of almost 40%. The negative bias of ISCCP relative to ind-SOBS is seasonally dependent, being more negative in winter by about 8% than in summer. Nighttime ISCCP results are biased by about 3%–6% more than daytime results, especially in summer/autumn, and exhibit larger standard deviations by about 6%. Both ind-SOBS and ISCCP are expected to underestimate cloud amount at night (see discussion in section 4c).

The shape of the difference distribution in Fig. 1 presents several puzzles. 1) There is an unusually large population near zero difference in cloud amount. 2) The very large standard deviation is caused by a small number of cases with very large differences (±50%–100%) in cloud amount. 3) The bias is caused solely by the asymmetry in the number of negative and pos-

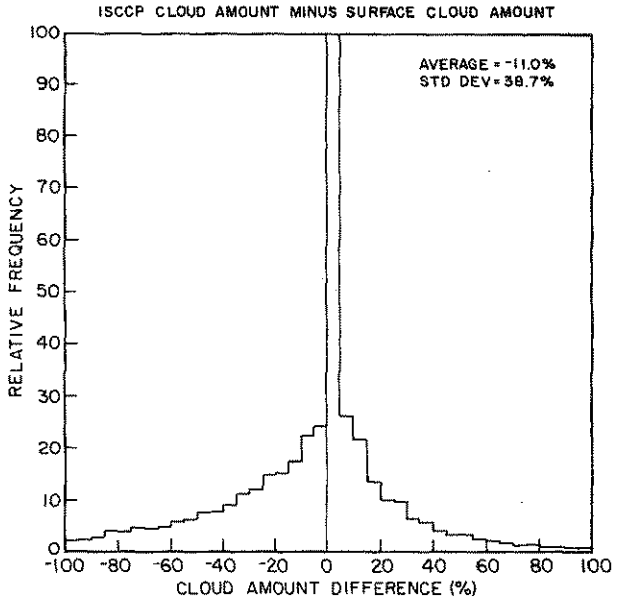

FIG. 1. Frequency distribution of differences between individual land surface weather station cloud amounts (three-hourly in octas converted to percent) and retrieved ISCCP cloud amounts (three-hourly, averaged over an equal area grid equivalent to 2.5° resolution at the equator). If more than one surface station is present in the ISCCP grid, one value is selected randomly. Results are for all available surface station reports for January 1984, July 1985, and October 1986 (over 670 000 cases).

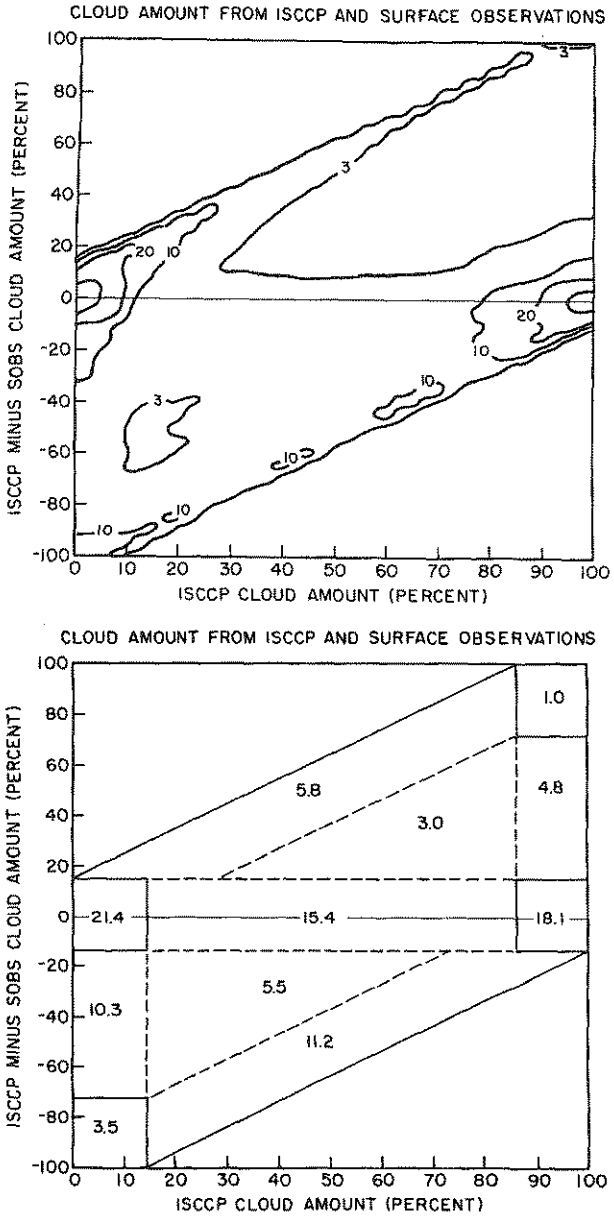

FIG. 3. (a) Differences shown in Fig. 1 plotted against the ISCCP cloud amount. Contours indicate frequencies in percent relative to the maximum value; the innermost (unlabeled) contours near (zero, zero) and (zero, 100%) indicate a relative frequency of 50%. (b) Percentage of the total population within each indicated subregion of the diagram in part (a).

in Fig. 2. Thus, the large population of zero differences in cloud amount in Fig. 1 is a consequence of the large frequency of either completely clear or completely overcast cases.

Figure 3 also shows that the extreme "wings" in the distribution in Fig. 1 are highly correlated with the total cloud amount, forming two slanting branches, one that goes from zero difference and zero cloud amount toward +100% difference and 100% cloud amount (in Fig. 3b: 5.8%) and one that goes from zero difference and 100% cloud amount toward −100% difference and zero cloud amount (Fig. 3b: 11.2%). These two branches also arise from the frequent occurrence of completely clear or completely overcast conditions but are produced by the comparison of two "perfect" cloud datasets, which observe very different sized areas (ind-SOBS represent areas that are about 5%–10% of the area covered by ISCCP). If the surface observations represented "perfect point measurements" of cloud amount, reporting only 0% and 100%, and they are compared to "perfect area measurements," then the pattern shown in Fig. 3a would necessarily result. Whenever the area is covered uniformly (cloud amount = 0% or 100%), the point measurement would always have the same value as the area measurement; this would cause the two peaks at zero difference and 0% and 100% cloud amount as already explained. Whenever the area is partially covered by a solid cloud layer, then the point measurements would always differ by the maximum possible amount, since the point values can only be 0% or 100%. For a large number of comparisons of areas to points located randomly within them (as done here), the number of cases with positive and negative differences would vary with the fraction of the area covered by cloud. For example, if 20% of the area is covered by cloud, the chances of a randomly located point measurement being either 0% or 100% would be 80% and 20%, respectively. If we remove from the lower branch in Fig. 3b a small population (about 4%–5%) that is similar in distribution to the differences between the two cloud amount distributions at low values shown in Fig. 2, representing a tendency for the ISCCP analysis to miss some clouds completely, then the ratio of the number of cases occurring in the two branches in Fig. 3a varies as a function of cloud amount just as predicted by this argument. Thus, the general shape of Fig. 1 (spike at zero difference and extreme "wings") is produced by comparing two "perfect" cloud measurements representing very different area sizes, where one measurement represents an area much smaller than the typical area covered by a cloud.

This supposition is confirmed by two additional results. First, we compared matched pairs of ind-SOBS observations located within individual ISCCP map grid cells. The resulting cloud amount difference distribution (Fig. 4) has the same shape and standard deviation as Fig. 1, but without the bias. Thus, cloud amounts reported at nearby surface sites can disagree by the maximum possible amount as expected from the discussion above. Second, we repeated the comparison of ind-SOBS to ISCCP for grid cells containing at least five surface reports; but instead of selecting one ind-SOBS value for comparison, we averaged three or five values. The resulting standard deviations of the differences decrease by about 7% and 10%, respectively. Thus, the large differences in individual cloud amounts in the wings of the distribution do not represent actual

different areas. The remaining standard deviation amount is associated with the error in estimating fractional area cover.

The overall summary of the results presented in Figs. 1, 2, and 3, based on the interpretation given above, is that individual ISCCP and ind-SOBS measurements of cloud amount agree to within about 15% in over 60% of the cases, with differences of about 25% for the cases with small-scale broken cloudiness (about 20% of the cases). In about 15% of the cases, there are larger disagreements because of the very large difference in the areas observed by the two systems; but, since these cases are caused by partial cover by large-scale clouds, this does not indicate any large errors in the ISCCP results. In about 5% of the cases, the ISCCP results report clouds not reported by the surface observer, whereas in about 15% of the cases, the ISCCP does not report clouds reported by the surface observer. At least half of these cases may be caused by the overreporting of 1 and 7 octas by the surface observers. Adding the detection errors to the last entry in Table 2, we estimate the instantaneous ISCCP cloud amounts at 280-km scale to be biased by about −10% with an rms uncertainty of about 25% over land. Thus, the two largest sources of error in the ISCCP results are detection errors (causing most of the bias and about half of the remaining standard deviation in the differences) and errors in estimating fractional area coverage by counting pixels (causing the other half of the remaining standard deviation).

b. *Effect of subpixel cloud variations*

Determination of cloud areal coverage by counting the number of satellite image pixels that contain cloud produces errors when broken cloudiness is composed of many individual cloud elements that are smaller than the satellite field of view (cf. Coakley and Bretherton 1982). There have been many assessments of the effect of image pixel size on cloud cover determinations [see references in Rossow et al. (1985), Rossow et al. (1989), Wielicki and Parker (1992)], but almost all of these studies examine the worst cases, namely, fair weather, boundary-layer cloudiness. The most thorough study of these worst cases (Wielicki and Parker 1992) shows that, at the pixel sizes used by ISCCP, the average bias in cloud cover is $\leq +5\%$ for low-level cloudiness; however, there are three other conclusions from this work that are equally important.

First, there are significant variations of optical thicknesses within the smaller-scale clouds, such that the transition from cloudy to clear conditions is represented by very small differences in measured radiances (~1%–2% in VIS and 1–2 K in IR) and occurs over a finite distance. This is especially true for marine boundary-layer clouds (Wielicki and Parker 1992); transitions are somewhat sharper over land (Parker et al. 1986). Kuo et al. (1988) illustrate the same continuum of cloud reflectances for cirrus. The main implication is that the threshold selected to divide cloudy and clear portions of an image is ambiguous and somewhat arbitrary, regardless of the spatial resolution of the data. In other words, the definition of "cloudy" is not entirely clear (cf. Rossow 1989) and the magnitude of changes in cloud amount produced by changing spatial resolution depends on the threshold used to make the cloudy–clear distinction and on the type of clouds considered (Wielicki and Parker 1992). Neglect of this optical thickness effect in earlier studies of the resolution dependence of cloud amounts caused a significant overestimate of the magnitude of the effect (Wielicki and Parker 1992).

Second, the rather small average overestimate of broken cloud amounts found by Wielicki and Parker is actually caused by two offsetting effects. The actual sensitivity of the cloud amounts determined with the ISCCP thresholds to changes in spatial resolution from $1/18 + 1$ km to 8 km is an increase of cloud amount by 10%–15% as resolution decreases (for boundary-layer cumulus), with most of the change occurring at pixel sizes >1 km. At the highest resolutions, however, the thresholds used by ISCCP underestimate total cloud amount because some very optically thin clouds are missed altogether. This effect also causes a systematic underestimate of the very thin cirrus clouds (optical thickness of the missed clouds is only a few tenths) examined by Wielicki and Parker, which exhibit little dependence on spatial resolution.

Third, the average bias error arises from much larger (20%–30%), but partly random, errors for specific cases (we discuss the reasons for this below). The result is only a small bias that depends on both the threshold magnitudes and image pixel size. Wielicki and Parker (1992) recommend thresholds over ocean of 5% for VIS and 3 K for IR for 8-km resolution. Since the resolution of ISCCP data varies from 4 to 7 km and the threshold values are 3% for VIS and 2.5 K for IR, the estimated overestimate for marine boundary-layer clouds is <5%.

For the cases where both the ISCCP and ground observers report partial cloud cover (in Fig. 3b: 3.0% + 15.4% + 5.5%), the two observations agree to within about 25% (Table 2). This magnitude of rms error is consistent with that found by Wielicki and Parker (1992), for individual 8-km pixels. One analysis of all-sky camera photographs shows a very high correlation (>0.8) of overhead cloud amount with cloud amount over the whole dome (Willand and Steeves 1991), which suggests that there is a preponderance of clouds with scales larger than about 2–3 km over the eastern United States. If broken cloudiness is generally at a scale (say 2–6 km) similar to the satellite pixel sizes, it would explain the good agreement between the satellite and ground observer measurements. Nevertheless, fair weather boundary-layer clouds do exhibit size distri-

4. Comparison to other cloud climatologies

a. Global, regional, and seasonal comparisons

Table 3 summarizes average cloud amounts for a variety of time and space domains from four cloud climatologies. The differences between the values are summarized in the last column by the rms differences of the values shown, calculated with and without the *Nimbus-7* results. In general, the ISCCP, SOBS, and METEOR total cloud amounts are very similar with global annual mean values >60%; the *Nimbus-7* cloud amount is about 9% less (cf. Stowe et al. 1989; Mokhov and Schlesinger 1993). Regional and seasonal cloud amounts differ among the four climatologies by <10%, except for the polar regions and the ocean. If the *Nimbus-7* results are excluded, then the differences are generally <6%, except for the polar regions, southern land areas, and oceans at night. The results for polar regions will be discussed in section 4d. The large difference between *Nimbus-7* and the other cloud amounts over oceans is directly attributable to the larger detection threshold used in the *Nimbus-7* analysis (about three times the ISCCP threshold), which lowers its sensitivity to low-level clouds. This interpretation is supported by the fact that the largest cloud amount differences occur in regions dominated by marine stratus and by the improvement in the agreement between the ISCCP and *Nimbus-7* results when the ISCCP thresholds are increased by a factor of 2 [Stowe et al. (1989) illustrate this effect on monthly zonal mean cloud amounts]. The effective detection threshold for the METEOR results has not been documented; however, the METEOR ocean cloud amounts generally lie between the ISCCP and *Nimbus-7* amounts.

Table 3 shows that the ISCCP cloud amounts are generally about 5% higher than the SOBS amounts over oceans, but are almost 10% larger than SOBS amounts over midlatitude oceans and over oceans at night (nighttime differences will be discussed in section 4c and large differences near sea ice margins and over the summer Arctic Ocean will be discussed in section 4d). This result occurs despite evidence that some clouds may be missed because of cloud contamination of the ISCCP clear radiances (Rossow and Garder 1993b). Warren et al. (1986, 1988) discuss several sources of bias error in the SOBS data over oceans. The systematic difference between the sky cover observed from the surface and the earth cover observed from satellite is expected to be very small over oceans because of the more horizontally homogeneous conditions (Warren et al. 1988). The weather bias is caused by ships trying to avoid foul weather, emphasizing fair weather conditions in the observations, but this is offset by ships spending more time in foul weather because of larger winds and waves. There is also an observer bias because the ship observers are not generally as well trained as land weather station observers. The weather bias is estimated to be about −0.4%, but may be as large as −2%, and the observer bias is estimated to be about −1.4% (comprised of an overestimate of cumulus cloud amounts and underestimates of stratus and cirrus cloud amounts). The underestimate of cirrus may be much larger at night and may be enhanced in daytime by the presence of more extensive low cloudiness, by hazier boundary layers over oceans, and by a tendency for observers to report cirrus only when an associated convective system is in view (Warren 1990, personal communication).

Figure 6 shows the zonal mean differences between the ISCCP and SOBS cloud amounts over land (upper panel) and ocean (lower panel), averaged over June–July–August (boreal summer) and December–January–February (boreal winter). The structure (two peaks) of the small differences near the equator over oceans suggests that the ITCZ as observed from satellites extends to higher latitudes than observed from the surface, consistent with an underreporting of cirrus cloud over oceans when it is far from the convective systems.

The large systematic differences in midlatitude cloudiness over oceans have a different geographic distribution (Fig. 7) and seasonal dependence in the two hemispheres. The Southern Hemisphere difference is about the same magnitude in all seasons and at most longitudes. The variation of differences in the Indian Ocean is caused by a weak zenith angle dependence of the ISCCP cloud amounts (Rossow and Garder 1993b). The zenith angle effect cannot account for all of the difference between ISCCP and SOBS cloud amounts, but it can account for the smaller differences between ISCCP and METEOR results. The METEOR results confirm higher cloud amounts in southern midlatitude oceans (Mokhov and Schlesinger 1993). Histograms of SOBS monthly cloud amount anomalies over the southern midlatitude oceans (difference of monthly mean and long-term mean values) show a standard deviation of about 15%, which is about half the estimated sampling error for a single observation (Warren et al. 1988), about twice the value obtained for SOBS data in northern midlatitude oceans, and twice the values obtained from all three satellite datasets for both hemispheres. Such a large standard deviation suggests that the SOBS results over southern oceans are less reliable because of a small sample size. The systematic difference in cloud amount may also be associated with a larger than usual weather bias in this area.

The Northern Hemisphere difference in ocean cloud amounts is comprised of a summer difference only in the Atlantic and a winter difference located along the equatorward edge of the storm-track zone, similar to the Southern Hemisphere difference (Fig. 7). The North Atlantic difference in summer cloud amount is located along the east coast of North America. This cloud difference pattern is consistent with the storm-track and low surface pressure anomaly patterns as-

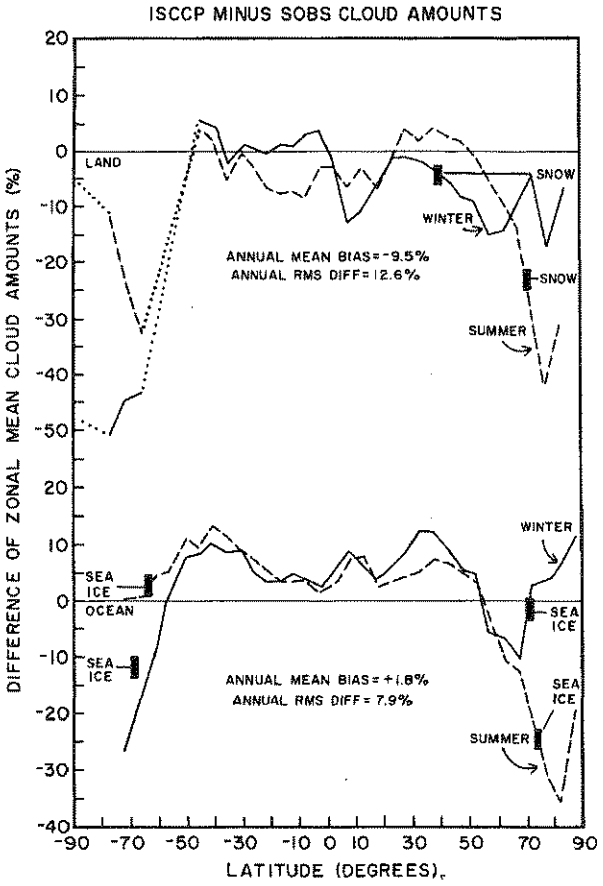

FIG. 6. Zonal mean differences in monthly mean cloud amounts between ISCCP results and the surface observations climatology (SOBS) of Warren et al. (1986, 1988) over land (upper panel) and ocean (lower panel), averaged over summer (June, July, August—dashed lines) and winter (December, January, February—solid lines). Equatorward extents of snow cover and sea ice cover in these two seasons are indicated by small black bars. Monthly results for ISCCP cover the period 1984–1988; results for SOBS cover the period 1971–1981.

average bias expected between satellite and SOBS cloud amounts is no more than 5%. This is consistent with the small negative bias in ISCCP cloud cover relative to surface observations when broken clouds are isolated (cf. section 3, Table 2). A more recent study by Henderson-Sellers and McGuffie (1990) suggests that this source of bias is smaller in practice, which is also consistent with our results when all cloud types are included in the comparison (Table 2). The larger negative bias of ISCCP cloud amounts over land in winter (Fig. 6) is consistent with the interpretation that the detection errors in ISCCP cloud amounts can explain general differences with SOBS of 5%–10%.

The geographic distribution of the differences in ISCCP and SOBS cloud amounts (Figs. 6 and 7) highlight three particular regions of larger differences: high-latitude land areas in Asia in winter, subtropical and tropical Africa, and the Caspian–Aral seas area. Although the ISCCP results underestimate winter cloud amounts somewhat more (cf. Table 2), because of more variable surface temperatures and reflectances and reduced infrared and visible radiance contrasts, the larger differences shown in Fig. 7 over Asia may be due partly to real changes in cloudiness between the 1970s and 1980s. Such large differences do not appear in the comparison between ISCCP and METEOR cloud amounts (Mokhov and Schlesinger 1993). Several other climate indicators also exhibit changes between these two decades: snow cover (Robinson and Dewey 1990), lower-tropospheric humidity (Gaffen et al. 1991), surface pressure patterns (Trenberth 1990), and surface temperatures (Hansen and Lebedeff 1988). The surface temperature and cloud amount changes, in particular, appear to have similar geographic features. The cloud amount differences over Africa (and the differences in dry season cloudiness over central South America) may be associated with the more severe drought conditions in the 1980s than during the 1970s (Nicholson 1989; Ward 1992). The larger ISCCP summer cloudiness near the Caspian and Aral seas may indicate increased dustiness caused by poor land management practices in this area (almost all of the ISCCP cloudiness present there is very warm and optically thin).

b. Cloud type comparison

To test whether the regional cloud amount differences between ISCCP and SOBS in Fig. 7 are associated with difficulties in observing particular cloud types, we sort the differences into categories defined by the mean cloud optical thickness and cloud-top pressure determined by ISCCP (Table 4). When predominantly low-level clouds are present over oceans, their detection with satellite IR radiances is difficult (e.g., Wielicki and Coakley 1981). During daytime conditions, VIS radiance tests overcome this limitation, accounting for the persistent difference of about 10% between the IR and VIS/IR cloud amounts over oceans. This effect also explains the even smaller ocean cloud amounts obtained from *Nimbus-7* results, which were obtained using a larger IR threshold than used by ISCCP. In general over oceans (Table 4), the ISCCP results indicate smaller cloud amounts than SOBS for low-level clouds and larger cloud amounts than SOBS for high-level clouds. These results are consistent with the ten-

FIG. 7. Geographic distribution of differences in (a) summer and (b) winter mean cloud amounts between ISCCP and SOBS (covering the same periods as indicated in Fig. 6). Heavy solid contour indicates zero difference, thin solid contours indicate larger ISCCP cloud amounts, and dashed contours indicate larger SOBS cloud amounts.

dency noted by Warren et al. (1988) for untrained ship observers to overestimate cumulus cloud amounts, to underestimate stratus cloud amounts, and to underestimate the amount of altocumulus cloudiness. These results also support the suggestion that ship observers underestimate cirrus cloud amounts.

Over land, the ISCCP cloud amounts are generally smaller than the SOBS amounts, with the largest differences for optically thin, middle- and upper-level clouds. The underestimate of the thinner clouds, which are detected primarily by the IR threshold test, is caused partly by the overly large IR threshold used.

c. *Day/night comparison*

Table 5 summarizes differences in day and night cloud amounts from three climatologies (the METEOR dataset has no information on day/night variations), where the *Nimbus-7* results are from local noon and midnight (without UV radiance tests), while the SOBS and ISCCP results are averages over three-hourly observations. The ISCCP results in Table 5 (and Table 3) have been corrected for the difference in sensitivity to low-level clouds between the VIS/IR detection algorithm and the IR-only algorithm by adding to the nighttime (IR only) cloud amounts the difference of the VIS/IR and IR-only cloud amounts interpolated in local time from the daytime results. Over oceans where the diurnal variation of surface temperature is very small, this correction procedure should work well; over land, where surface temperature decreases at night, this correction may be underestimated. The magnitude of this correction to ISCCP cloud amounts is indicated in Table 5 by the values in parentheses, which show the uncorrected nighttime cloud amounts (see also the parenthetical values in Table 3). This correction does not alter the phase of diurnal cloud variations in the ISCCP dataset. The *Nimbus-7* results shown in Table 5 are based on an IR-only analysis; the values in parentheses show the day–night cloud amount differences using the IR/UV algorithm during daytime and the IR-only algorithm at night.

There is no agreement even on the sign of the day–night cloud amount contrast. Surface observers have more difficulty identifying cloudiness at night, particularly higher-level clouds, and are expected to underestimate nighttime cloud amounts (Warren et al. 1986). This detection bias is also expected to be larger over oceans than land because low-level stratus are more frequent (Warren et al. 1988). Comparing observations on moonlit nights to those with less illumination suggests underestimates of 3%–5% over land and 5%–10% over oceans (Hahn et al. 1993). Globally and annually (Table 3), there is almost no difference in day/night cloud amount in the ISCCP results, however, this lack of difference results from canceling land–water and seasonal variations. Over land, daytime cloud amounts are larger by 3% in winter and 6% in summer; over ocean, nighttime cloud amounts are larger by about 2% in all seasons. SOBS results, if corrected for variations of nighttime illumination, may confirm a larger daytime than nighttime cloud amount over land, but with a difference that is smaller in magnitude than ISCCP, and may show a slightly larger nighttime than daytime cloud amount over oceans.

d. *Polar cloudiness*

Table 3 and Fig. 6 show very large differences in polar cloud amounts, which have also been found in other datasets (Hughes 1984; Key and Barry 1989; Rossow and Lacis 1990; Curry and Ebert 1992; Schweiger and Key 1992; Mokhov and Schlesinger 1993). Comparison of the three satellite climatologies shows a different relationship among them for polar regions than for the rest of the globe (Table 3): the *Nimbus-7* cloud amounts are usually lower than the METEOR and ISCCP values, but they are higher than both in the polar regions (Mokhov and Schlesinger 1993). All the satellite values are lower than SOBS cloud amounts in the polar regions.

Figure 8 compares the annual cycle of cloud amount from ISCCP and SOBS, averaged over different latitude ranges for the North and South poles, and illustrates recently proposed revisions of the surface climatology. Curry and Ebert (1992) argue that "diamond dust," a form of ice precipitation that occurs mostly in polar winter, is not counted as cloud by surface observers even though optical thicknesses >5 have been observed from aircraft (Curry et al. 1990). They estimate that winter cloud amounts in the central Arctic are similar to summer cloud amounts [based on Huschke (1969) and Warren et al. (1986), (1988)].

Similar large disagreements occur over Antarctica in winter. The winter SOBS values at the South Pole are suspect because the frequency of monthly mean values that are precisely equal to the long-term climatological value is about five times larger than any other value, suggesting a large number of bogus reports. Schneider et al. (1989) find that reported cloud amounts at the South Pole in winter are highly correlated with lunar (actually sky) brightness (cf. Hahn et al. 1993). Using the observed linear relationship, they estimate the corrections to winter cloud amounts shown in Fig. 8, leaving little annual variation in cloud amount. Most of the cloud that is missed during winter is "nonopaque" (Schneider et al. 1989). Similar corrections are presumably needed for the Arctic as well.

ISCCP (and the other satellite) analyses underestimate cloud amounts at both poles by about 10% in winter [but see discussion in Schweiger and Key (1992) of *Nimbus-7* and ISCCP wintertime values] and at least 25% in summer. This assessment is supported by preliminary analyses using other spectral channels on

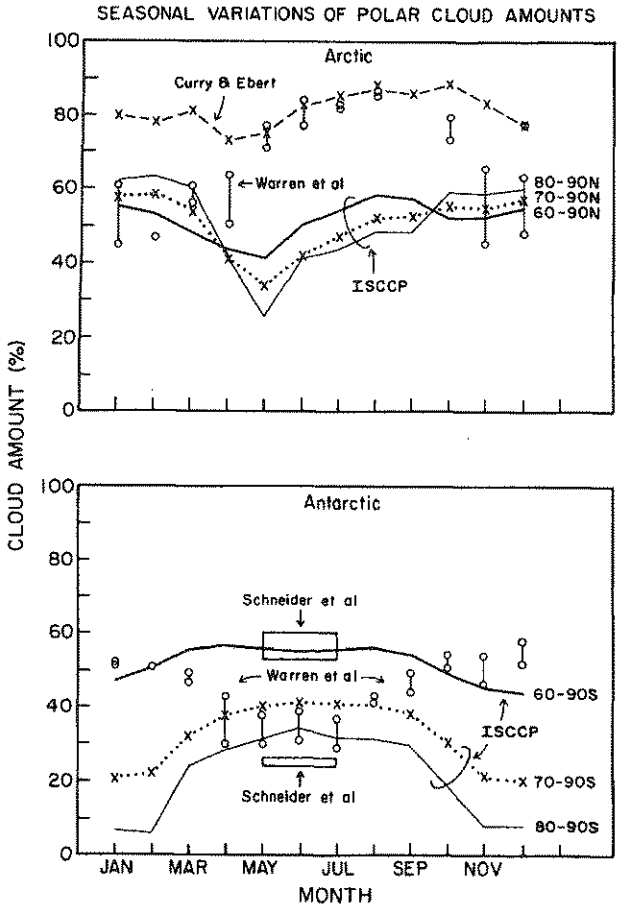

FIG. 8. Comparisons of the seasonal variations of average cloud amount in the (a) Arctic and (b) Antarctic determined by ISCCP and other cloud climatologies. The climatology of Warren et al. (1986, 1988) is represented by connected open circles, where the upper circle represents an average over 60°–90°N in the Arctic and 60°–90°S in the Antarctic and the lower circle represents near-polar values. The average cloud amounts in the central Arctic, adopted from Huschke (1969) by Curry and Ebert (1993), are shown by dashes in (a). Corrections to winter South Polar cloud amounts proposed by Schneider et al. (1989) are indicated by open bars in (b), where the lower bar represents opaque clouds and the upper bar represents total cloudiness.

of cloud amount. Well-known features are readily apparent: three zonal bands of high cloud amount, one within about 10° of the equator, and one in each hemisphere between 30° and 60° latitude (Fig. 10a). The cloud band in southern midlatitudes is the most nearly continuous, whereas the other two bands are interrupted over land areas. Land areas are generally less cloudy than ocean areas at all latitudes; the difference in average cloudiness in the two polar regions is also consistent with this distinction.

The seasonal cycle (approximately represented by the second and third PCs) accounts for about 14% of the total variance. The spatial pattern of the seasonal cycle shows that it is dominated by tropical variations and that the phases of the tropical and midlatitude seasonal changes oppose one another (cf. Rossow and Lacis 1990). The larger variation (second PC) is in phase with the solstice seasons while the third PC is in phase with the equinoctal seasons. The fact that it takes two PCs to represent the seasonal oscillation is indicative of significant asymmetries in the time variations (see, e.g., Mitchell and Wallace 1992).

Table 7 compares the results of an EOF analysis of the ISCCP, SOBS, METEOR, and *Nimbus-7* cloud climatologies by showing the amount of variance found in each of the first six PCs and aggregated for all higher-order PCs, as well as the correlations of the spatial maps for the first four PCs. The quantitative agreement of both the spatial maps and the amount of variance explained is excellent (cf. Mokhov and Schlesinger 1993), with the exception of the amount of variance accounted for by the first PC in SOBS data. The fact that there is so much variance in higher-order PCs for SOBS and that the amount of variance is constant over all higher PCs suggests that the SOBS results have much more variance that behaves like "white noise," which may be due to the very sparse coverage over oceans and the Southern Hemisphere. The much larger interannual variability determined from SOBS for southern midlatitudes (Table 6) supports this idea. If we rescale the relative variances by the total contained in the first six PCs (numbers in parentheses), we get much better agreement. SOBS also agrees less well on the spatial patterns because of poor coverage of the Southern Hemispheric oceans.

The results in Table 7 suggest good agreement among the datasets for the first three PCs, but not the fourth one; the first three PCs account for about 80% of the variations in the three satellite datasets and about 60% of the variations in SOBS (or 94% of the variance in the first six PCs). Thus, the features of the cloud distribution that we can confirm are the annual mean geographic distribution (with the polar regions somewhat more uncertain) and the amplitude and phase of the seasonal variations.

5. Discussion

a. Uncertainty in ISCCP cloud amounts

The uncertainty in a single determination of cloud amount comes from four sources: 1) estimation of fractional area coverage, 2) area sampling, 3) time sampling, and 4) detection errors.

1) When we isolate small-scale broken cloud cases in the comparison between ISCCP and ind-SOBS, we find a small ($\approx$4%) negative bias that is consistent with other estimates of the difference between "sky cover" and "earth cover" (Warren et al. 1986). We also find an rms difference of about 25% that is consistent with studies of the effects of finite satellite resolution on determination of fractional cover (Wielicki and Parker 1992). The magnitude of errors in single pixels is probably larger still; however, the variations of cloud

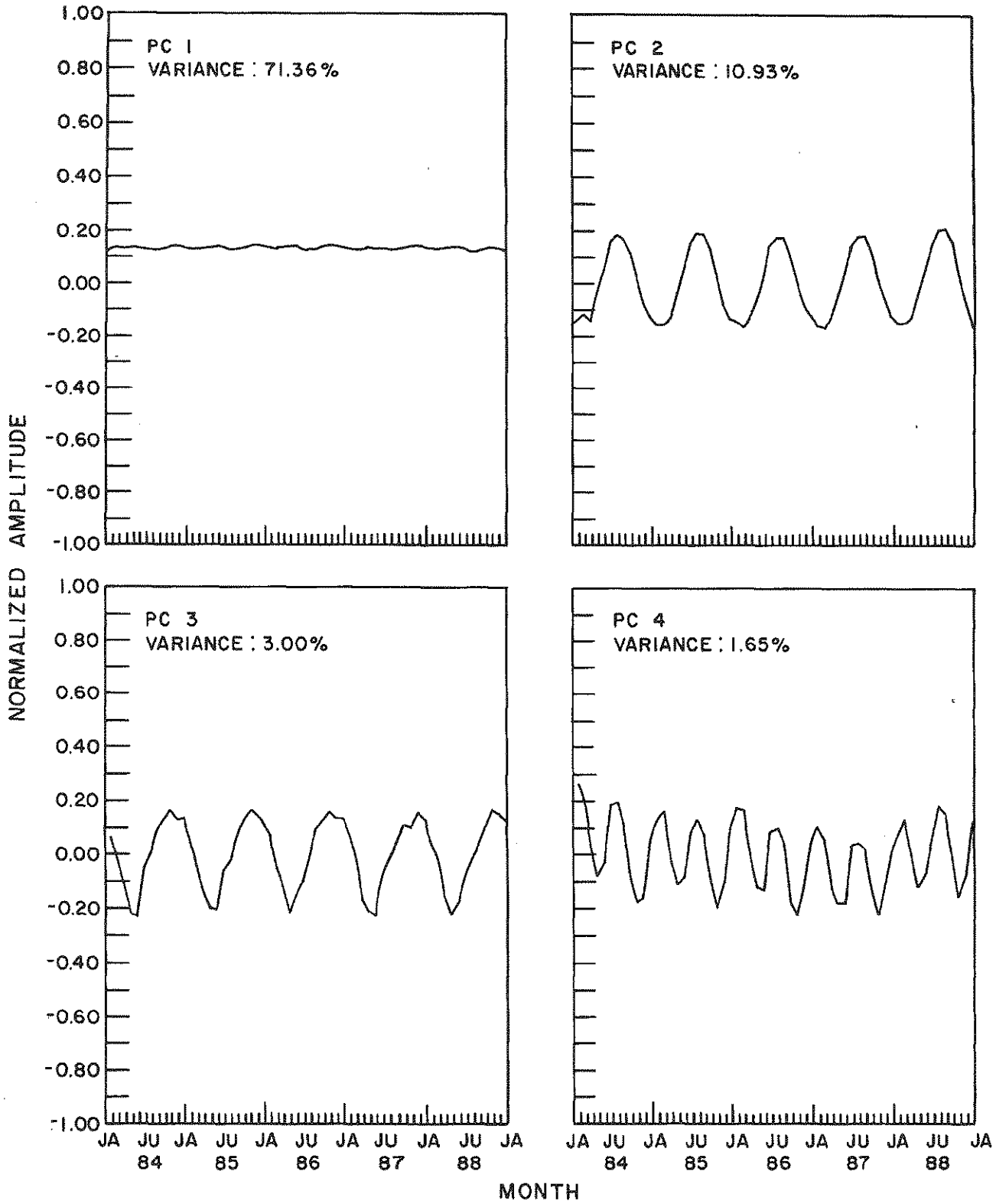

FIG. 9. First four eigenvectors (time variations) for monthly mean cloud amounts determined by EOF analysis from ISCCP results on an equal-area map grid equivalent to 5° × 10° resolution at the equator and covering the period 1984–1988. Fraction of the total variance explained by each principal component is indicated.

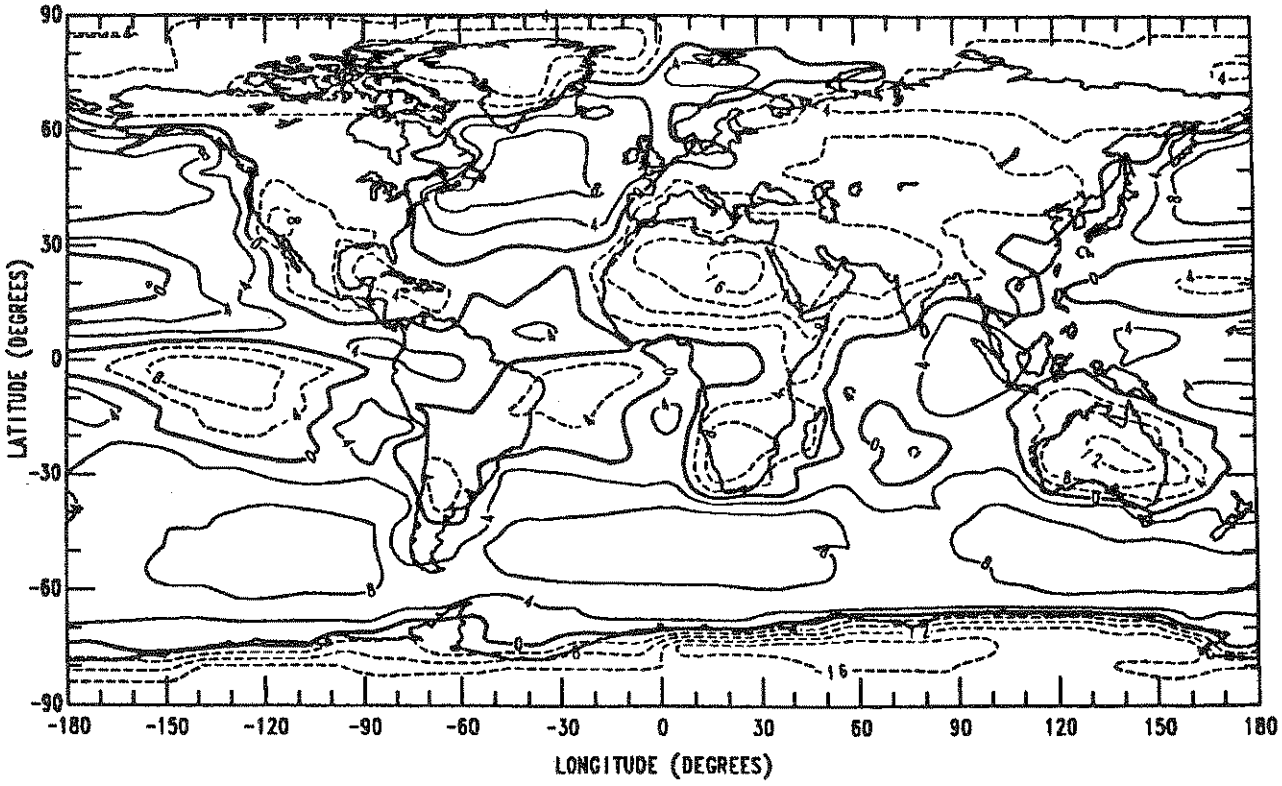
90
60
30
0
-30
-60
-90
LATITUDE (DEGREES)
-180 -150 -120 -90 -60 -30 0 30 60 90 120 150 180
LONGITUDE (DEGREES)

a

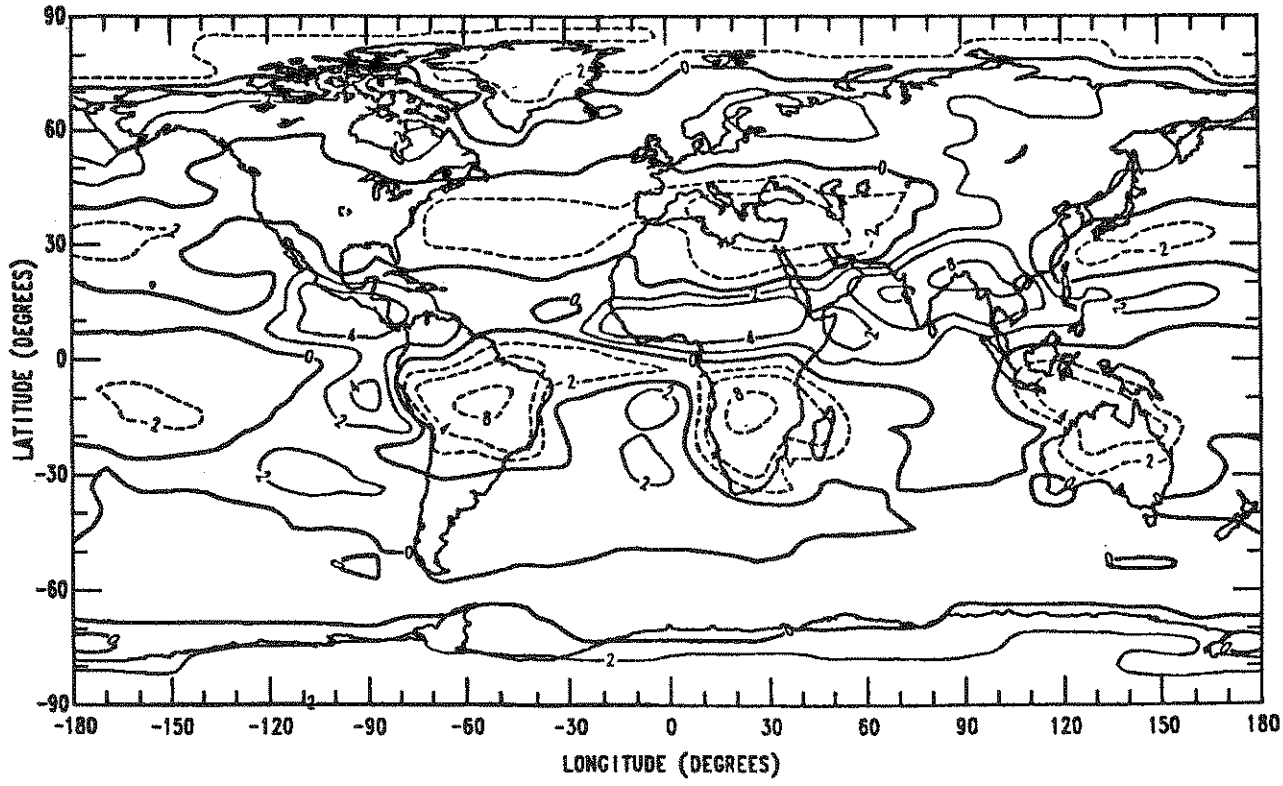
90
60
30
0
-30
-60
-90
LATITUDE (DEGREES)
-180 -150 -120 -90 -60 -30 0 30 60 90 120 150 180
LONGITUDE (DEGREES)

b

of cloud amount on time scales from 3 h to 8 yr (July 1983 through June 1991).[7] This dataset has more uniform coverage of the whole globe at all times of day with the densest sampling, thereby minimizing the uncertainties associated with spatial and temporal sampling. Much work by many researchers will be required to examine these data thoroughly and determine the meaningful behavior of clouds. We have presented only some simple summaries. Some notable features of the cloud distribution are listed below (cf. Table 3).

1) The global annual mean cloud amount is about 63% and exhibits little (<1% rms) variation from month to month. Over the whole 8-yr ISCCP record, the global annual mean cloud amount has undergone a slow cycle, apparently associated with El Niño occurrences, with an amplitude of ±4%.

2) The mean annual Southern Hemisphere cloud amount is almost 6% larger than the mean Northern Hemisphere cloud amount; the mean western hemisphere cloud amount is a little more than 4% larger than the eastern hemisphere cloud amount. Both of these facts arise from a systematic difference between the average cloud amount over ocean and land and from the differences in hemispheric land fractions. The mean annual ocean cloud amount is about 23% larger than the land cloud amount (the ISCCP results probably overestimate this difference by 5%–10%).

3) If each hemisphere is divided into latitude zones of 30° width, the middle zone (30°–60°) has the largest mean cloud amount in the ISCCP results, about 10% larger than the global mean value. However, the average cloud amount of the tropical–subtropical zone is a combination of smaller (than global mean) subtropical cloud amounts and larger cloud amounts in the tropics. Consequently, the largest latitudinal contrast in cloud amount occurs between the tropics and subtropics. Since both the ISCCP and SOBS results underestimate polar cloudiness, the polar regions may actually have slightly larger cloud amounts than middle latitudes.

4) The land/ocean differences in mean cloud amount imply longitudinal contrasts of cloudiness that are as large as the latitudinal contrasts. The largest contrasts occur in the subtropics between land deserts and marine stratocumulus regimes near the west coasts of continents.

5) The seasonal variation of global mean cloud amount is very small (<0.5%); however, this occurs because of cancellation of seasonal changes between lower and middle latitudes (all climatologies show large seasonal variations at polar latitudes, but these may be exaggerated by detection errors) and between the Northern and Southern hemispheres. Low-latitude cloud amounts are largest in summer, while middle-latitude cloud amounts are largest in winter. The amplitude of the seasonal cloud amount variations is larger in the Northern Hemisphere because seasonal variations are larger over land than oceans.

6) In the ISCCP results there is almost no difference in global and annual mean cloud amounts between daytime and nighttime; however, this occurs because of cancellation between land and ocean diurnal variations. Mean cloud amounts are larger during nighttime than during daytime over oceans and larger during daytime than during nighttime over land. Most of the diurnal variation of cloud amounts over oceans occurs at lower latitudes. Over middle-latitude land the amplitude of the diurnal variation of cloud amount is about twice as large in summer as in winter.

Acknowledgments. This work has benefited from discussions with a large number of colleagues over the years. We wish to thank participants in the algorithm intercomparison studies, particularly A. Arking, J. Coakley, M. Desbois, E. Harrison, P. Minnis, F. Mosher, E. Raschke, E. Ruprecht, G. Sèze, and E. Smith. We wish to highlight the contributions of G. Sèze who worked with us on the crucial final designs; her work on time variations of the radiances was key to use of this concept in the cloud algorithm. We also thank B. Barkstrom, F. Bretherton, G. Gutman, A. Henderson-Sellers, T. Inoue, J. Key, J. London, R. Saunders, M. Schlesinger, A. Slingo, G. Stephens, L. Stowe, and T. Vonder Haar for thoughtful comments and B. Wielicki and D. Wylie for an ongoing conversation about the meaning of "cloud." ISCCP is the first project of the World Climate Research Program. During organization and operations of ISCCP, P. Morel was director of the Joint Planning Staff for WCRP at WMO and T. Kaneshige (succeeded by S. Benedict) was the staff member responsible for coordinating ISCCP meetings and reports. The international project manager and source of our funding for ISCCP is Dr. Robert Schiffer (NASA). Drafting was done by L. Del Valle and word processing by C. Koizumi; we thank them for their excellent support.

APPENDIX

ISCCP Participants

ISCCP data processing has been accomplished by the combined efforts of several institutions, which are listed here along with their representatives (in chronological order). The capture of original satellite datasets, quality checking, and their reduction by sampling are performed by the sector processing centers (SPC). For NOAA polar orbiters, the SPC is the National Oceanic and Atmospheric Administration (represented by G. Hunolt, H. Jacobowitz, H. Drahos, J. Gibson, M. Mignono, and K. Kidwell). For Meteosat, the SPC is the European Space Agency (ESA) (R.

[7] ISCCP data collection, processing, and analysis is planned to continue through at least 2000.

Sèze, G., and W. B. Rossow, 1991: Effects of satellite data resolution on measuring the space-time variations of surfaces and clouds. *Int. J. Remote Sens.*, **12**, 921–952.

——, F. Drake, M. Desbois, and A. Henderson-Sellers, 1986: Total and low cloud amounts over France and southern Britain in the summer of 1983: Comparison of surface-observed and satellite-retrieved values. *Int. J. Remote Sens.*, **7**, 1031–1050.

Stowe, L. L., C. G. Wellemeyer, T. F. Eck, H. Y. M. Yeh, and the NIMBUS-7 Cloud Data Processing Team, 1988: NIMBUS-7 global cloud climatology. Part I: Algorithms and validation. *J. Climate*, **1**, 445–470.

——, H. T. M. Yeh, T. F. Eck, C. G. Wellemeyer, H. L. Kyle, and the NIMBUS-7 Cloud Data Processing Team, 1989: NIMBUS-7 global cloud climatology. Part II: First year results. *J. Climate*, **2**, 671–709.

Trenberth, K. E., 1990: Recent observed interdecadal climate changes in the Northern Hemisphere. *Bull. Amer. Meteor. Soc.*, **71**, 988–993.

Ward, M. N., 1992: Provisionally corrected surface wind data, worldwide ocean–atmosphere surface fields, and Sahelian rainfall variability. *J. Climate*, **5**, 454–475.

Warren, S. G., C. J. Hahn, J. London, R. M. Chervin, and R. L. Jenne, 1986: Global distribution of total cloud and cloud type amounts over land. NCAR Tech. Note TN-273 + STR/DOE Tech. Rep. ER/60085-HI, 29 pp. + 200 maps. [NTIS number DE87-00-6903].

——, ——, ——, ——, and ——, 1988: Global distribution of total cloud and cloud type amounts over the ocean. NCAR Tech. Note TN-317 + STR/DOE Tech. Rep. ER-0406, 42 pp. + 170 maps. [NTIS number DE90-00-3187].

Welch, R. M., K. S. Kuo, B. A. Wielicki, S. K. Sengupta, and L. Parker, 1988: Marine stratocumulus cloud fields off the coast of southern California observed using LANDSAT imagery. Part I: Structural characteristics. *J. Appl. Meteor.*, **27**, 341–362.

Wielicki, B. A., and J. A. Coakley, 1981: Cloud retrieval using infrared sounder data: Error analysis. *J. Appl. Meteor.*, **20**, 157–169.

——, and R. M. Welch, 1986: Cumulus cloud field properties derived using LANDSAT digital data. *J. Climate Appl. Meteor.*, **25**, 261–276.

——, and L. Parker, 1992: On the determination of cloud cover from satellite sensors: The effect of sensor spatial resolution. *J. Geophys. Res.*, **97**, 12 799–12 823.

Willand, J. H., and J. Steeves, 1991: Sky-cover correlation within a sky dome. *J. Appl. Meteor.*, **30**, 1037–1039.

Yamanouchi, T., and S. Kawaguchi, 1992: Cloud distribution in the Antarctic from AVHRR data and radiation measurements at the surface. *Int. J. Remote Sensing*, **13**, 111–127.